

Mapping key soil micronutrients across the Tibetan Plateau

Huangyu Huo^{1,2}, Xiling Gu^{1,2}, Jiayi Li^{1,2}, Shanshan Yang¹, Yafeng Wang^{1*}, Jinzhi Ding^{1*}

¹State Key Laboratory of Tibetan Plateau Earth System, Environment and Resources (TPESER), Institute of Tibetan Plateau Research, Chinese Academy of Sciences, Beijing 100101, China.

²University of Chinese Academy of Sciences, College of Resources and Environment, Beijing 100049, China.

*Corresponding to: Jinzhi Ding (jzding@itpcas.ac.cn), Yafeng Wang (yfwang@itpcas.ac.cn)

Abstract. Soil micronutrients supply sustains critical ecological functions but exhibit poorly quantified distribution patterns in high-altitude ecosystems. This study bridges this knowledge gap through a large-scale investigation across the Tibetan Plateau, a cold-arid region where cryogenic weathering, aridity, and suppressed pedogenesis interact to govern micronutrient cycling. We assembled a plateau-wide dataset from 526 sites with triplicate surface soils (0-10 cm) per site (n = 1,660). ~~Seven-Four~~ micronutrients (Fe, Mn, ~~Cu, Zn, Ni, and V, Mo~~) were measured and paired with multi-source predictors (climate, vegetation, soil ~~properties~~~~covariates~~, topography, ~~grazing~~ disturbance, and weathering proxy). Elemental contents span broad ranges, with site-level summaries (mean \pm SD, mg·kg⁻¹) of Fe 22,864.30 \pm 7,589.01, Mn 576.74 \pm 206.44, ~~Cu 25.32 \pm 9.28~~, Zn 27.24 \pm 8.55, ~~and Ni 49.35 \pm 10.98~~, V 56.99 \pm 19.33, ~~and Mo 4.63 \pm 1.14~~. Random Forest model was employed to quantify controls and generate high-resolution spatial maps. Key results reveal that pronounced regional heterogeneity is driven primarily by weathering intensity with secondary modulation from climate and topography covariates. ~~Key results reveal that pronounced regional heterogeneity driven primarily by climate related weathering intensity and topography variable, with secondary modulation from soil and vegetation factors.~~ Element-specific spatial patterns were observed, with Fe enrichment in southeastern/southern plateaus, Mn gradients increasing southeastward ~~and Cu over the western northern plateau with minima in the southeast.~~ Zn hotspots in central-eastern and western marginal zones, ~~Ni enriched across the northern central interior and western highlands~~, and V exhibits a moderate spatial gradient, with higher contents in the southeastern Tibetan Plateau and relatively lower values in the northwest. ~~Mo weakly patterned, slightly higher on northern basins and lower toward the southeast.~~ We provide 1-km maps of all ~~sevenfour~~ micronutrients together with pixel-wise uncertainty layers to support benchmarking of process-based micronutrient cycling models and to inform sustainable ecosystem management under climate change. The dataset is openly available at TPDC (<https://doi.org/10.11888/ Terre.tpd.303049303242>; Huo et al., 2025).

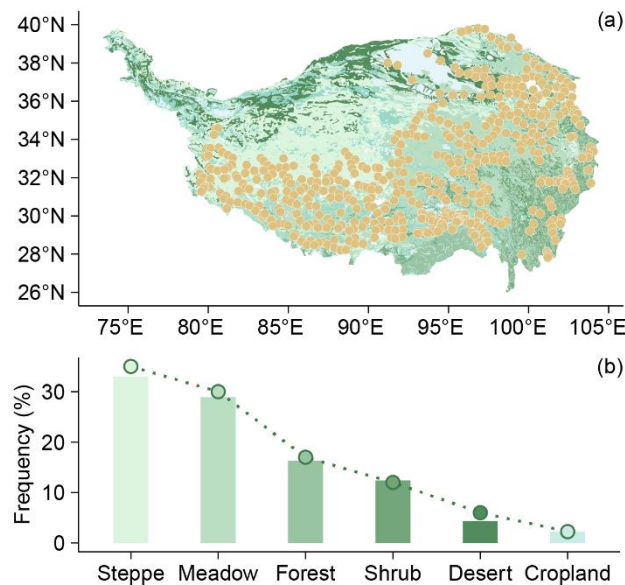
27 **1 Introduction**

28 As essential yet trace-level components of living systems, micronutrients (e.g., Fe, Mn, ~~Cu~~, Zn, ~~Ni~~, and V, ~~Mo~~) sustain
29 fundamental ecological processes, including photosynthesis (Fe, Mn; Fischer et al., 2015; Schmidt et al., 2020), respiration
30 (Fe; Dallman, 1986), enzymatic/redox functions (~~Cu~~, Zn, ~~Mn~~, V; Hänsch et al., 2009), and biological nitrogen fixation (~~Ni~~, V,
31 ~~Mo~~; O'Hara, 2001). Crucially, micronutrient gradients in soils propagate through trophic chains, directly influencing human
32 nutrition and health; deficiencies exacerbate global malnutrition burdens (Fageria et al., 2002; White et al., 2005). Despite
33 their pivotal role in ecosystem stability and food security (Presteele et al., 2016; Stehfest et al., 2019), critical knowledge
34 gaps persist regarding the distribution patterns and drivers of soil micronutrients from regional to global scales.

35 The Tibetan Plateau represents a uniquely important yet underrepresented region for addressing these knowledge gaps. As
36 the high-altitude landmass and the most extensive alpine permafrost region at low to mid-latitude (Yao et al., 2012), the
37 Tibetan Plateau supports vast areas of cold- and nutrient-limited ecosystems, where plant productivity, microbial activity, and
38 biogeochemical cycling are particularly sensitive to micronutrient availability (Han et al., 2022; Tian et al., 2019). In such
39 environments, micronutrients may act as co-limiting or even primary limiting factors alongside nitrogen and phosphorus, yet
40 their spatial distributions and environmental controls remain poorly quantified (Dong et al., 2023; Pan et al., 2024).
41 Moreover, the Tibetan Plateau is experiencing rapid climate change characterized by accelerated warming and increasing
42 moisture availability, which is expected to fundamentally alter soil weathering regimes, redox conditions, and
43 mineral-organic interactions (Yu et al., 2024; Cheng et al., 2024). Without robust baseline assessments of soil micronutrients,
44 it remains difficult to evaluate how ongoing climate change may reshape nutrient limitation patterns and ecosystem
45 functioning across high-altitude regions.

46 Soil micronutrient supply originates from coupled physicochemical weathering and biological mediation, critically regulated
47 by local climate and topography (Ochoa-Hueso et al., 2020; Hartmann et al., 2023). In cold-arid high-altitude regions,
48 particularly the Tibetan Plateau, extreme environmental interactions uniquely govern micronutrient cycling. Cryogenic
49 processes such as glacial erosion and freeze-thaw cycles, accelerate physical bedrock weathering to mobilize lithogenic
50 micronutrient reservoirs, while aridity concurrently constrains chemical weathering and elemental release (Mu et al., 2020;
51 Mu et al., 2016). Low temperatures suppress biological turnover and synergize with aridity to compromise pedogenesis
52 through clay deficits and diminished mineral reactive sites, thereby reducing elemental retention capacity (Dijkstra et al.,
53 2004). The combined effects of these opposing processes jointly determine the overall abundance and spatial heterogeneity
54 of soil micronutrients across alpine soils, likely differing from the patterns of soil micronutrients observed in temperate and
55 tropical regions. These counteracting processes fundamentally shape micronutrients distribution patterns, yet remain severely

56 understudied. Current research is largely restricted to localized transects (e.g., Heihe River Basin, Tibetan Plateau Highway)
57 with limited spatial representation (Zhang et al., 2012; Guan et al., 2017; Bu et al., 2016).
58 Despite the ecological significance of soil micronutrient, our understanding of their spatial distribution and controlling
59 factors across the Tibetan Plateau remains limited. Previous studies have been largely confined to localized transects or
60 site-specific investigations (e.g., the Heihe River Basin and the Tibetan Plateau Highway), offering limited spatial coverage
61 and representativeness, and providing insufficient insight into how climate, vegetation, topography and lithology jointly
62 regulate micronutrient patterns at the regional scale (Zhang et al., 2012; Guan et al., 2017; Bu et al., 2016). To address these
63 knowledge gaps, we conducted a large-scale field investigation across the Tibetan Plateau, establishing 526 sampling sites
64 distributed across representative temperature and moisture gradients (Fig. 1). The sampling design encompassed the plateau's
65 dominant vegetation types and lithological classes. Using this dataset, we analyzed distribution patterns and key controlling
66 factors for seven essential micronutrients (Fe, Mn, Cu, Zn, Ni, V, Mo). We then applied a Random Forest algorithm to
67 generate high-resolution spatial distribution maps of these micronutrients, representing the first comprehensive
68 quantification at this scale and resolution.



69 **Figure 1.** Sampling strategy and ecosystem representativeness. (a) Spatial distribution of sampling sites superimposed on China's
70 1:1,000,000 vegetation map. (b) Areal proportions of ecosystem types (bars) versus sampling point frequency distribution (dots) across
71 corresponding ecosystems. Similar bar and dot heights indicate that the sampling is proportionally representative.
72

73 2 Methods

74 2.1 Field survey and soil micronutrients analysis

75 We analyzed 1,660 topsoil samples collected from 526 locations during a 2019-2021 growing season (July-August) field
76 survey across the Tibetan Plateau (79-105°E, 27-40°N; **Fig. 1a**). Sampling sites represent major plateau ecosystems: forests,
77 shrubs, steppes, meadows, deserts, and croplands (**Table 1**). Our field sampling followed a proportional, area-weighted
78 design, whereby the number of sampling sites allocated to each ecosystem type was approximately proportional to its areal
79 extent across the Tibetan Plateau. This design aims to provide a plateau-wide, regionally representative characterization of
80 surface-soil micronutrients across dominant ecosystem types. The sites span broad environmental gradients, ranging from
81 759 to 5565 m in elevation, -7.83 to 18.46 °C in mean annual temperature (MAT), and 23 to 898 mm in mean annual
82 precipitation (MAP), effectively capturing the plateau's topographic and climatic variability. Site was selected using
83 standardized criteria: maintaining relative homogeneity in species composition, community structure, and habitat conditions,
84 and avoiding proximity to roads or areas with frequent human activity. At each site, we established a 10*10 m² quadrat and
85 collected triplicate soil samples along the diagonal at three positions (0 m, 7.1 m, and 14.1 m; 0-10cm depth), corresponding
86 to the start, midpoint, and end of the quadrat diagonal. This design allows sampling across the spatial heterogeneity within
87 each plot while maintaining a standardized sampling framework.~~At each location, we established a 15 m transect collecting~~
88 ~~triplicate soil samples (0-10 cm depth) at 0 m, 7.5 m, and 15 m positions.~~ This depth was chosen because it represents the
89 biologically active surface horizon most relevant to plant uptake and microbially mediated cycling, and is widely used in
90 regional soil inventories for comparability across ecosystems (Du et al., 2017; Cardon et al., 2013). ~~On the Tibetan Plateau,~~
91 ~~steppes and meadows constitute the dominant land cover, so most samples correspond to mineral A horizons; in forested sites,~~
92 ~~the 0-10 cm layer may include an organic rich surface.~~ This consistent protocol ensures cross-site comparability while
93 capturing the variability of surface layer that most strongly interacts with vegetation and climate. Geographic coordinates,
94 elevation, community type, and species composition (Cheng et al., 2022) were systematically documented.
95 To ensure the reliability of soil micronutrient measurements, we adopted a two-step analytical strategy. First, all 1,660
96 topsoil samples collected from 526 sampling locations were air-dried, sieved (2 mm), and analyzed in the laboratory using a
97 third-generation X-ray fluorescence spectrometer (XRF). All micronutrient data reported in this study are based on these
98 laboratory XRF measurements. Second, to independently validate the XRF-derived concentrations, a subset of 218 samples
99 was randomly selected and re-analyzed using inductively coupled plasma-mass spectrometry (ICP-MS), a widely accepted
100 reference method for elemental analysis (Simon, 2005). Among the examined elements, Fe ($R^2 = 0.81$), Mn ($R^2 = 0.67$), Zn
101 ($R^2 = 0.49$), and V ($R^2 = 0.77$) exhibit clear and statistically significant linear relationships with ICP measurements,
102 demonstrating moderate to strong correlation (Fig. S1). The increased dispersion observed at low contents reflects known
103 limitations of XRF near detection thresholds, rather than method failure. Moreover, our analytical strategy follows
104 established practice in large-scale geochemical mapping, where XRF is commonly used for high-throughput determination

of total/major-element composition, while ICP-based methods are commonly employed in parallel for complementary measurements (e.g., extracted fractions, waters, or elements requiring lower detection limits) and, where appropriate, for inter-method comparison and validation. In addition to GEMAS and the NGSAs, similar XRF-based workflows have been implemented in other regional/national baseline programmes (e.g., BGS G-BASE in the UK, the FOREGS Geochemical Atlas of Europe, and the Global Geochemical Baselines framework). These precedents support the robustness and suitability of using XRF with targeted ICP verification for plateau-scale geochemical datasets (Table S1).

To ensure the reliability of soil micronutrient measurements, we adopted a two-step analytical strategy. First, in situ measurements were conducted using a second-generation portable Niton X-ray fluorescence (XRF) analyzer to obtain preliminary contents under natural field conditions. However, because this instrument could not reliably detect Mo, all soil samples were subsequently air-dried, sieved (2 mm), and re-analyzed in the laboratory using a third-generation XRF. Compared with the second-generation device, the third-generation XRF offers an extended detection range and improved accuracy (Lemière, 2018). All data presented in this study are based on the laboratory XRF measurements.

To further validate the laboratory XRF results, a subset of 218 samples was randomly selected and re-analyzed using Inductively coupled plasma Mass Spectrometry (ICP-MS), a widely accepted reference method (Simon, 2005). The two methods showed strong correlations for Fe, Mn, Cu and V ($R^2 = 0.67-0.89$, $P < 0.001$), with values closely aligning with the 1:1 line, indicating reliable quantification. For Zn and Ni, XRF and ICP-MS results were also significantly correlated, though systematic deviations from the 1:1 line were observed (Fig. S1). XRF tended to slightly over- or underestimate absolute contents of Zn and Ni compared with ICP-MS. To address this, we calibrated Zn and Ni, using the regression relationships between the two methods and then repeated spatial mapping. For Mo, the results obtained from the two methods were not fully consistent, likely due to its low content. Comparative results of both methods are provided in the Supplementary Information (Figs. S2-S4).

Table 1. Ecosystem classification and sampling coverage on the Tibetan Plateau.

Biome	Characteristics and dominant plant species	elevation ranges	climate conditions (temperature/precipitation)	No. of samples	No. of locations
Steppe	Alpine steppes, dominated by cold-adapted herbaceous species such as <i>Stipa purpurea</i> , features sparse vegetation adapted to cold-arid conditions.	1961-5151 m	-7.1-8.0 °C; 34.32-785.61 mm	569	180
Meadow	Alpine meadows feature dense, low-stature vegetation sustained by year-round low temperatures, high humidity, and water-retentive soils. These ecosystems thrive on gentle slopes and valley floors at higher elevations, hosting relatively diverse flora with characteristic dominance of sedges including <i>Kobresia pygmaea</i> and <i>K. humilis</i> .	2661-5565 m	-7.8-9.2 °C; 158.42-848.70 mm	499	154

Forest	Forests on the Tibetan Plateau concentrate primarily in the southeastern region, dominated by high-altitude cold-temperate coniferous forests. These humid-adapted ecosystems feature <i>fir (Abies)</i> and <i>spruce (Picea)</i> species as characteristic components.	1453-4237 m	-0.6-16.5 °C; 400.34-898.48 mm	265	87
Shrub	Tibetan shrublands primarily occur in arid and alpine zones, characterized by low-growing, drought-tolerant dwarf shrubs such as <i>Lonicera (honeysuckle)</i> and <i>Rhododendron</i> species adapted to nutrient-poor soils and extreme climatic conditions.	2169-5022 m	-5.2-11.8 °C; 301.40-868.63 mm	190	64
Desert	Alpine deserts occur in extremely arid, cold regions and exhibit extremely sparse vegetation dominated by <i>arid-tolerant dwarf shrubs</i> and <i>herbs</i> .	2108-5158 m	-7.1-5.6 °C; 22.64-443.43 mm	101	29
Cropland	Cropland, concentrated in river valleys and basin floors and is dominated by highland barley (<i>Hordeum vulgare</i> var. <i>nudum</i> , “qingke”), with spring wheat (<i>Triticum aestivum</i>), rapeseed (<i>Brassica napus</i>), and potato (<i>Solanum tuberosum</i>) commonly cultivated; vegetation cover is strongly seasonal and often bare after harvest.	759-4360 m	0.5-18.4 °C; 112.53-783.06 mm	36	12

127 Biomes are grouped by diagnostic characteristics; dominant plant species are italicized. Elevation range gives the minimum-maximum
128 elevation (m) of sampling sites within each biome. Climate conditions report site-level ranges of mean annual temperature (°C) and mean
129 annual precipitation (mm). No. of samples is the number of soil samples analyzed (0-10 cm, three replicates per site), and No. of locations
130 is the number of unique sampling sites.

131 2.2 Soil Properties

132 Soil samples were sifted through 2 mm sieve, discarding visible stones and extracted roots. Soil pH was measured using the
133 potentiometric method, and soil texture analysis, quantifying clay, silt, and sand content fractions, was determined using a
134 laser diffraction particle size analyzer (Mastersizer 2000, Malvern, UK). ~~The sieved samples were air dried for elemental~~
135 ~~analysis.~~ Soil organic carbon (SOC) content was quantified via the potassium dichromate oxidation method (Walkley-Black)
136 with external heating. The chemical index of alteration (CIA) was calculated using the molar proportions of Al₂O₃, CaO*,
137 Na₂O, and K₂O according to the formula: $CIA = [Al_2O_3 / (Al_2O_3 + CaO^* + Na_2O + K_2O)] \times 100$ (Fedo et al., 1995). ~~The~~
138 ~~major-element oxides used to calculate CIA (Al₂O₃, CaO, Na₂O and K₂O) were obtained from laboratory XRF measurements,~~
139 ~~which provide a well-established basis for CIA-based evaluation of relative chemical weathering gradients, and data quality~~
140 ~~was ensured through standard QA/QC including replicate analyses and certified reference materials. The chemical index of~~
141 ~~alteration~~ CIA reflects the relative loss of mobile base cations (Ca, Na, K) compared with the enrichment of immobile Al
142 during weathering (McLennan, 1993). Higher ~~chemical index of alteration~~ CIA values indicate stronger chemical weathering
143 and more advanced soil development, whereas lower values suggest weaker weathering and limited leaching of base cations
144 (Nesbitt et al., 1982).

145 2.3 Environmental variables

146 We considered geographic, climatic, biological, and edaphic drivers. Field measurements provided location (longitude,
147 latitude), slope, aspect and vegetation type. For the spatial prediction of micronutrient distributions, however, the gridded
148 predictor variables (e.g., elevation, slope, aspect, vegetation cover) were derived from online datasets in order to upscale
149 site-level observations to the Plateau scale. Slope and aspect data came from the National Tibetan Plateau Data Center
150 (<https://data.tpdc.ac.cn>). The digital elevation model (DEM) data were collected from the Resource and Environment
151 Science and Data Center (<https://www.resdc.cn/>).—Climate variables, mean annual temperature (MAT) and mean annual
152 precipitation (MAP) were downloaded from the Climate Data Store (<https://cds.climate.copernicus.eu#!/home>). The Aridity
153 Index (AI), calculated as mean annual precipitation/mean annual reference evapotranspiration, was obtained from the Global
154 Aridity Index dataset (Trabucco et al., 2018), where higher values indicate greater humidity. Vegetation types (Forest, Shrub,
155 Meadow, Steppe, Desert, Cropland) followed the 1:1,000,000 China Vegetation Map classification (Hou, 2019). The
156 normalized difference vegetation index (NDVI) data were obtained from an Earthdata Search (<https://search.earthdata.nasa.gov/search>). The net primary productivity (NPP) data were obtained from the study by Chen et al. (2023) and
157 were calculated using the CASA model (Potter et al., 1993). The grazing activity data were obtained from statistical
158 yearbooks. Based on the lithological data published by Dijkshoorn et al. in 2018, the rock types on the Tibetan Plateau were
159 classified into acidic igneous rock (IA), acidic metamorphic rock (MA), clastic sedimentary rock (SC), carbonate rock (SO),
160 aeolian facies rock (UE), and fluvial facies rock (UF).

162 2.4 Relative importance analysis and soil micronutrient mapping

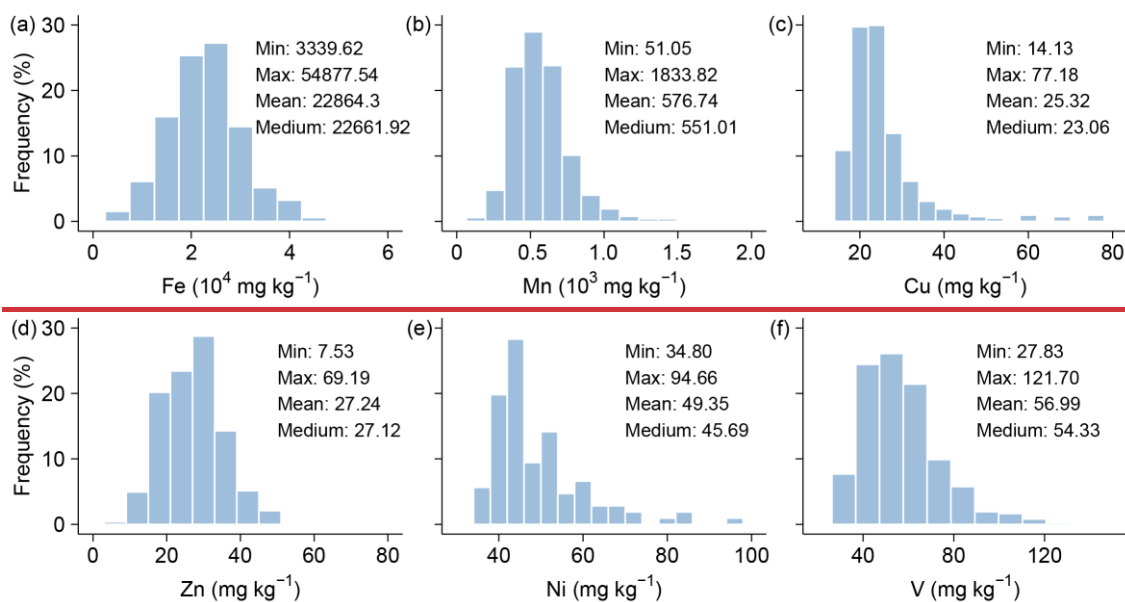
163 Soil micronutrient measurements were preprocessed to detect and remove outliers exceeding the mean \pm 3 standard
164 deviations. After data screening, the retained sample sizes are: Fe 1654 (from 1660), Mn 1630 (from 1646), ~~Cu 920 (from~~
165 ~~946)~~, Zn 1655 (from 1661), ~~Ni 180 (from 181)~~, and V 857 (from 867), ~~and Mo 120 (from 123)~~. To evaluate the relative
166 importance of predictors in explaining soil micronutrient variability across the Tibetan Plateau, we applied the random forest
167 permutation importance (%IncMSE) to independently cross-validate the driver rankings. For spatial prediction, we
168 developed ~~seven-four~~ area-wide random forest models (each comprising 500 trees) targeting Fe, Mn, ~~Cu, Zn, Ni, and V, and~~
169 ~~Mo~~ contents. The models were trained using a suite of environmental predictors, including topographic features (DEM, slope,
170 aspect), climate variables (MAT, MAP, AI), vegetation indices (NDVI, NPP), soil ~~covariates~~ properties (texture, SOC, pH,
171 CIA), and grazing intensity. Random forest was selected for its ability to model complex, nonlinear relationships and
172 interactions among diverse types of predictors. Model hyperparameters were optimized using grid search combined with
173 tenfold cross-validation. To assess model generalizability, we examined the extent to which the predictor parameter space in
174 the validation set overlapped with that of the original training data. Model performance was evaluated by comparing

175 predicted versus observed values using scatterplots (predicted on the x-axis, observed on the y-axis) following the method of
 176 Piñeiro et al. (2008), with models achieving strong predictive performance ($R^2 = 0.6-0.7$). The uncertainty layer is calculated
 177 as the inter-pixel variance among tree predictions. All spatial predictions were produced on a uniform 1 km grid (0.01°)
 178 across the Tibetan Plateau to maintain consistent spatial support for both predictions and associated uncertainty estimates.
 179 All statistical analyses were conducted using R version 3.4.4.

181 3 Results

182 3.1 Soil micronutrients contents

183 Across all sites, soil micronutrient contents varied widely, with mean value of $22,864.30 \pm 7,589.01$ for Fe (mean \pm SD,
 184 $\text{mg} \cdot \text{kg}^{-1}$), 576.74 ± 206.44 for Mn, 25.32 ± 9.28 for Cu, 27.24 ± 8.55 for Zn, 49.35 ± 10.98 for Ni, and 56.99 ± 19.33 for V,
 185 and 4.63 ± 1.14 for Mo. Coefficients of variation (CV = SD/mean) were 33% for Fe, 36% for Mn-, 37% for Cu, 31% for Zn,
 186 22% for Ni, and 34% for V and 25% for Mo. Collectively, Fe and Mn dominate in absolute abundance, whereas Cu-Zn and
 187 Ni-V occur at tens of $\text{mg} \cdot \text{kg}^{-1}$ and Mo remains low ($\sim 5 \text{ mg} \cdot \text{kg}^{-1}$), indicating heterogeneous but orderly micronutrient levels
 188 across the Plateau (Figs. 2 and S52).



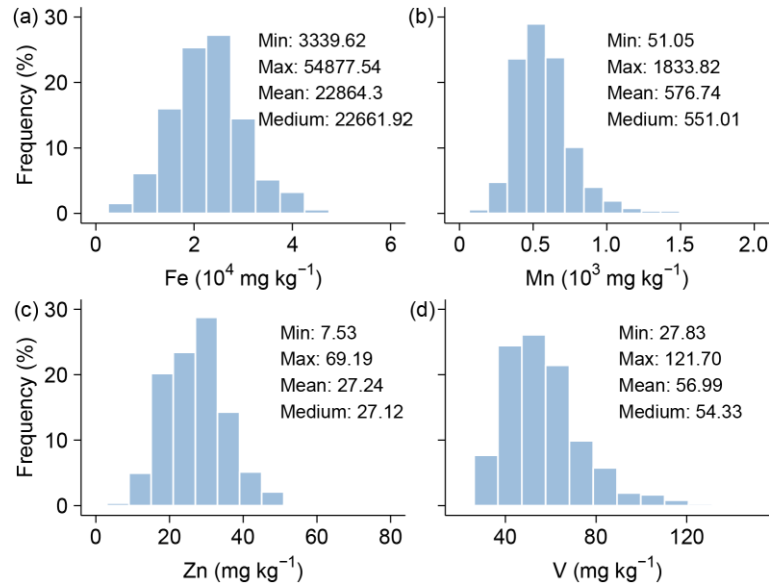


Figure 2. Frequency distributions of soil micronutrients (Fe, Mn, Cu, Zn, Ni, V) across the Tibetan Plateau.

3.2 Soil micronutrients across vegetation types

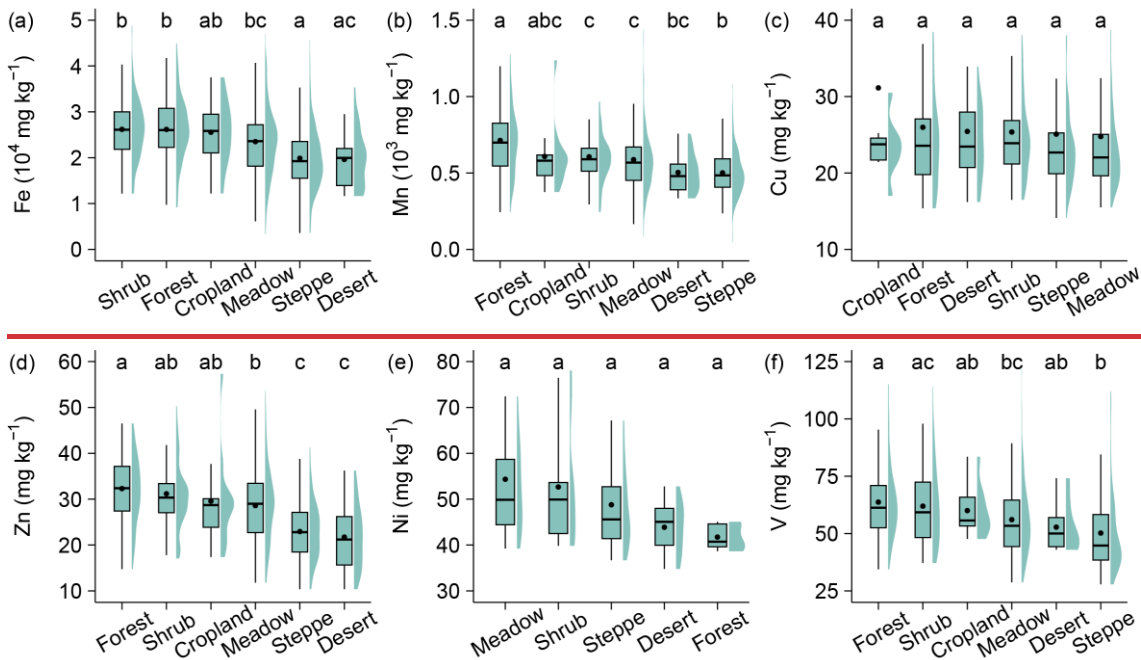
Soil micronutrient content (Fe, Mn, Zn, and V) varied significantly among different vegetation types (Fig. 3). Fe contents were highest in shrub and forest ecosystems, with mean values of $26,264.11 \text{ mg}\cdot\text{kg}^{-1}$ and $26,090.66 \text{ mg}\cdot\text{kg}^{-1}$, respectively, significantly exceeding values observed in desert ($19,762.66 \text{ mg}\cdot\text{kg}^{-1}$) and steppe ecosystems ($19,852.37 \text{ mg}\cdot\text{kg}^{-1}$) by 31-33%. Similarly, Mn contents were significantly higher in forest ($703.22 \text{ mg}\cdot\text{kg}^{-1}$) than in shrub ($606.33 \text{ mg}\cdot\text{kg}^{-1}$), meadow ($591.59 \text{ mg}\cdot\text{kg}^{-1}$), desert and steppe ecosystems (both below $510 \text{ mg}\cdot\text{kg}^{-1}$). Zn demonstrated a strong vegetation-dependent variability, with forest ($32.00 \text{ mg}\cdot\text{kg}^{-1}$) exhibiting the highest values and steppe ($22.94 \text{ mg}\cdot\text{kg}^{-1}$) and desert ($21.95 \text{ mg}\cdot\text{kg}^{-1}$) the lowest, shrub and cropland were intermediate and not significantly different from forest or meadow. V also varied among vegetation types, with forest being significantly higher than meadow and steppe, and shrub significantly higher than steppe, whereas cropland and desert displayed intermediate levels. Soil micronutrients contents (Fe, Mn, Cu, Zn, Ni, V, and Mo) varied significantly among different vegetation types (Figs. 3 and S6). Fe contents were highest in shrub and forest ecosystems, with mean values of $26,264.11 \text{ mg}\cdot\text{kg}^{-1}$ and $26,090.66 \text{ mg}\cdot\text{kg}^{-1}$, respectively, significantly exceeding values observed in desert ($19,762.66 \text{ mg}\cdot\text{kg}^{-1}$) and steppe ecosystems ($19,852.37 \text{ mg}\cdot\text{kg}^{-1}$) by 31-33%. Similarly, Mn contents were greatest in forest ($703.22 \text{ mg}\cdot\text{kg}^{-1}$) and cropland ($608.29 \text{ mg}\cdot\text{kg}^{-1}$), followed by shrub ($606.33 \text{ mg}\cdot\text{kg}^{-1}$) and meadow ($591.59 \text{ mg}\cdot\text{kg}^{-1}$), while the lowest Mn levels were recorded in desert and steppe ecosystems (both below $510 \text{ mg}\cdot\text{kg}^{-1}$). Soil Cu showed minimal variation across vegetation types, with mean values ranging narrowly between 25.23 and $31.14 \text{ mg}\cdot\text{kg}^{-1}$. Cropland had slightly higher Cu levels, but the differences were not statistically significant, suggesting a relatively

uniform spatial distribution of Cu across ecosystems. Zn, however, demonstrated a strong vegetation dependent variability, with the highest mean contents found in forest (32.00 mg·kg⁻¹) and shrub (31.15 mg·kg⁻¹) ecosystems. In contrast, Zn levels were markedly lower in steppe (22.94 mg·kg⁻¹) and desert (21.95 mg·kg⁻¹) soils, with differences exceeding 10 mg·kg⁻¹, indicating pronounced biogeochemical variation.

In contrast to the previous elements, Ni and Mo exhibited distinct patterns across vegetation types, with notably lower contents in forest and shrub ecosystems. Ni contents were highest in meadow soils (54.34 mg·kg⁻¹), followed by shrub (52.66 mg·kg⁻¹), steppe (48.78 mg·kg⁻¹), cropland (48.22 mg·kg⁻¹), desert (43.87 mg·kg⁻¹), and forest ecosystems (41.73 mg·kg⁻¹). Soil Mo contents showed negligible differences among ecosystems, though cropland exhibited marginally higher levels. No statistically significant differences were observed between vegetation types, indicating minimal vegetation control over Mo distribution.

The highest soil V mean value occurred in forest soils (63.70 mg·kg⁻¹), followed by shrub (61.94 mg·kg⁻¹) and cropland ecosystems (60.02 mg·kg⁻¹). These values were markedly greater than those observed in steppe (50.22 mg·kg⁻¹) and desert (52.80 mg·kg⁻¹) soils, with differences reaching up to 25%. Meadow soils showed intermediate V levels (56.07 mg·kg⁻¹).

Statistical comparisons revealed that V contents in forest and shrub ecosystems were significantly higher than those in steppe and meadow ecosystems ($p < 0.05$).



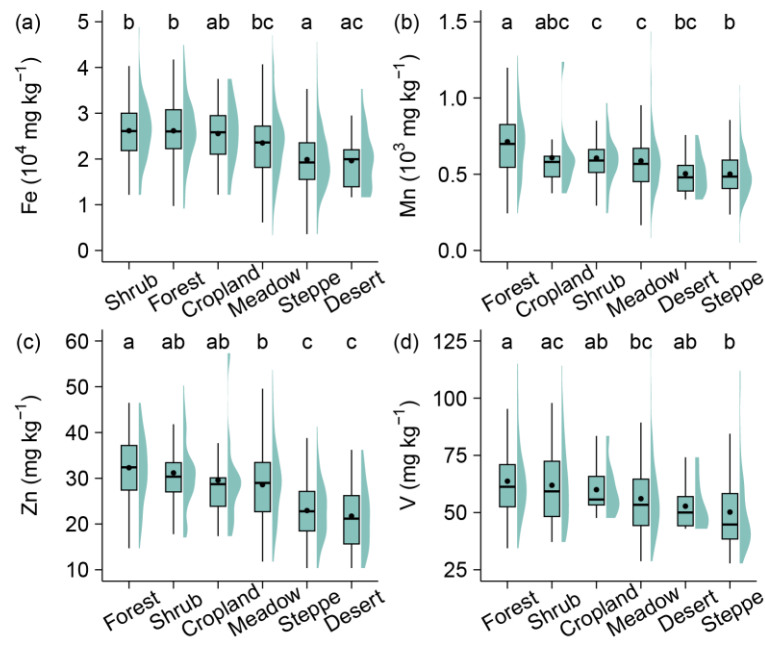
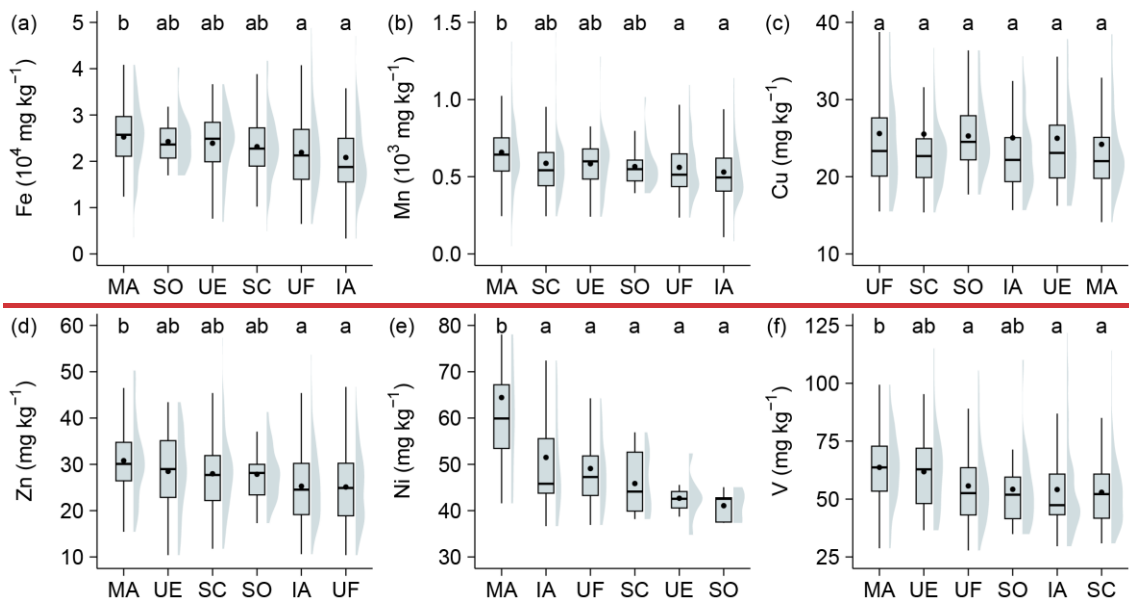


Figure 3. Variability in soil micronutrient contents (Fe, Mn, ~~Cu~~, Zn, ~~Ni~~, V) across Tibetan vegetation types. Boxplots show the data distributions for each vegetation type. Within each plot, the boxes represent the interquartile range (IQR), the horizontal lines within boxes indicate the median values, and black dots denote the mean values. The whiskers extend to 1.5 times the IQR. The surrounding shaded violin shapes indicate the kernel density distribution of the data. Lowercase letters denote significance groups from Tukey's HSD multiple comparisons ($\alpha = 0.05$): groups sharing at least one letter do not differ significantly, whereas groups with no letters in common differ significantly (e.g., "ab" is not different from "a" or "b").

3.3 Soil micronutrients across lithological classes

Lithological class exerted a significant influence on the distribution of several soil micronutrients (Fig. 4). Fe contents differed among lithological classes, with soils derived from acidic metamorphic rocks showing the highest mean value $25,252.72 \text{ mg}\cdot\text{kg}^{-1}$ and being significantly higher than soils developed from acidic igneous rocks ($20,830.15 \text{ mg}\cdot\text{kg}^{-1}$) and fluvial facies rocks ($21,910.22 \text{ mg}\cdot\text{kg}^{-1}$), whereas carbonate ($24,260.96 \text{ mg}\cdot\text{kg}^{-1}$), eolian facies ($23,902.77 \text{ mg}\cdot\text{kg}^{-1}$), and clastic sedimentary rocks ($23,157.66 \text{ mg}\cdot\text{kg}^{-1}$) exhibited intermediate levels and were not significantly different from either group. A similar pattern was observed for Mn, where acidic-metamorphic-driven soils ($658.37 \text{ mg}\cdot\text{kg}^{-1}$) were significantly higher than acidic-igneous-driven soils ($530.45 \text{ mg}\cdot\text{kg}^{-1}$) and fluvial-facies-driven soils ($560.91 \text{ mg}\cdot\text{kg}^{-1}$), with the remaining lithologies showing intermediate values. Zn also varied among lithologies, with the highest mean content in acidic metamorphic rocks ($30.79 \text{ mg}\cdot\text{kg}^{-1}$), which was significantly higher than acidic igneous rocks ($25.27 \text{ mg}\cdot\text{kg}^{-1}$) and fluvial facies rocks ($25.10 \text{ mg}\cdot\text{kg}^{-1}$), while eolian facies, clastic sedimentary, and carbonate rocks did not differ significantly from acidic metamorphic rocks or the lower group. For V, acidic-metamorphic-derived soils ($63.67 \text{ mg}\cdot\text{kg}^{-1}$) were significantly higher than fluvial facies, acidic igneous, and clastic sedimentary derived soils, whereas eolian facies rocks and carbonate rocks showed intermediate levels and were not significantly different from acidic metamorphic rocks or the lower group.

247 Lithological class exerted a significant influence on the spatial distribution of certain soil micronutrients (Figs. 4 and S7). Fe
 248 contents differed notably across lithological classes, with the highest values observed in soils derived from acidic
 249 metamorphic rocks (mean value: 25,252.72 mg·kg⁻¹), followed by those from carbonate rocks (24,260.96 mg·kg⁻¹) and
 250 eolian facies rocks (23,902.77 mg·kg⁻¹). The lowest Fe contents were recorded in soils developed from acidic igneous rocks
 251 (20,830.15 mg·kg⁻¹). A similar geochemical pattern was observed for Mn, with the maximum contents in
 252 acidic metamorphic driven soils (658.37 mg·kg⁻¹), and the lowest in acidic igneous driven soils (530.45 mg·kg⁻¹).
 253 Zn contents in soils also varied across lithologies, with the highest values associated with acidic metamorphic rocks (mean
 254 value of 30.79 mg·kg⁻¹), followed by eolian facies rocks and elastic sedimentary rocks, while relatively lower levels were
 255 found under acidic igneous rocks (25.27 mg·kg⁻¹) and fluvial facies rocks (25.10 mg·kg⁻¹). In contrast, Cu showed no
 256 significant differences among lithological classes. Cu contents were slightly higher under fluvial facies rocks (25.60
 257 mg·kg⁻¹), but overall differences were minimal. Similarly, Mo contents were relatively uniform, with slightly elevated levels
 258 under acidic metamorphic rocks and eolian facies rocks (both ~4.86 mg·kg⁻¹), and lower values under elastic sedimentary
 259 rocks and carbonate rocks (both <4.48 mg·kg⁻¹), though differences were not statistically significant.



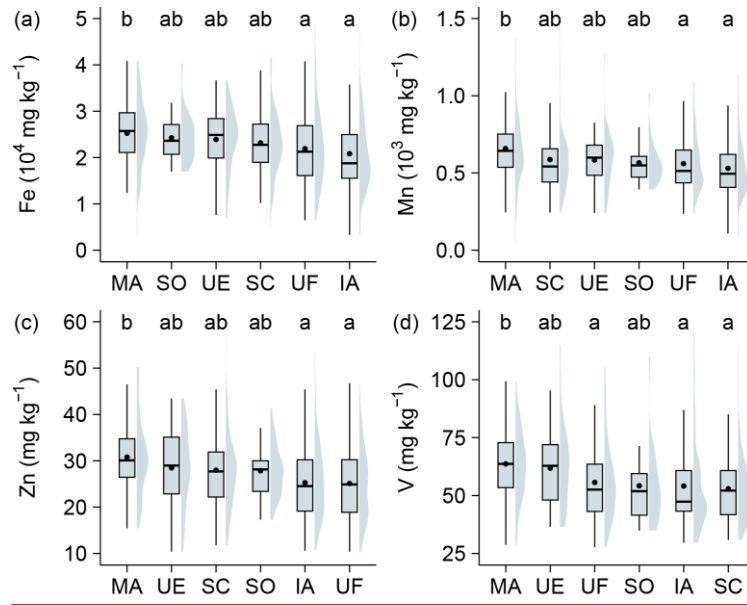


Figure 4. Variability in soil micronutrient contents (Fe, Mn, Cu, Zn, Ni, V) across Tibetan lithological classes. Boxplots show the data distributions for each lithological classes. Within each plot, the boxes represent the interquartile range (IQR), the horizontal lines within boxes indicate the median values, and black dots denote the mean values. The whiskers extend to 1.5 times the IQR. The surrounding shaded violin shapes indicate the kernel density distribution of the data. Lowercase letters denote significance groups from Tukey's HSD multiple comparisons ($\alpha = 0.05$): groups sharing at least one letter do not differ significantly, whereas groups with no letters in common differ significantly (e.g., "ab" is not different from "a" or "b"). Abbreviations of lithological classes: IA = acidic igneous rock, MA = acidic metamorphic rock, SC = clastic sedimentary rock, SO = carbonate rock, UE = eolian facies rock, UF = fluvial facies rock.

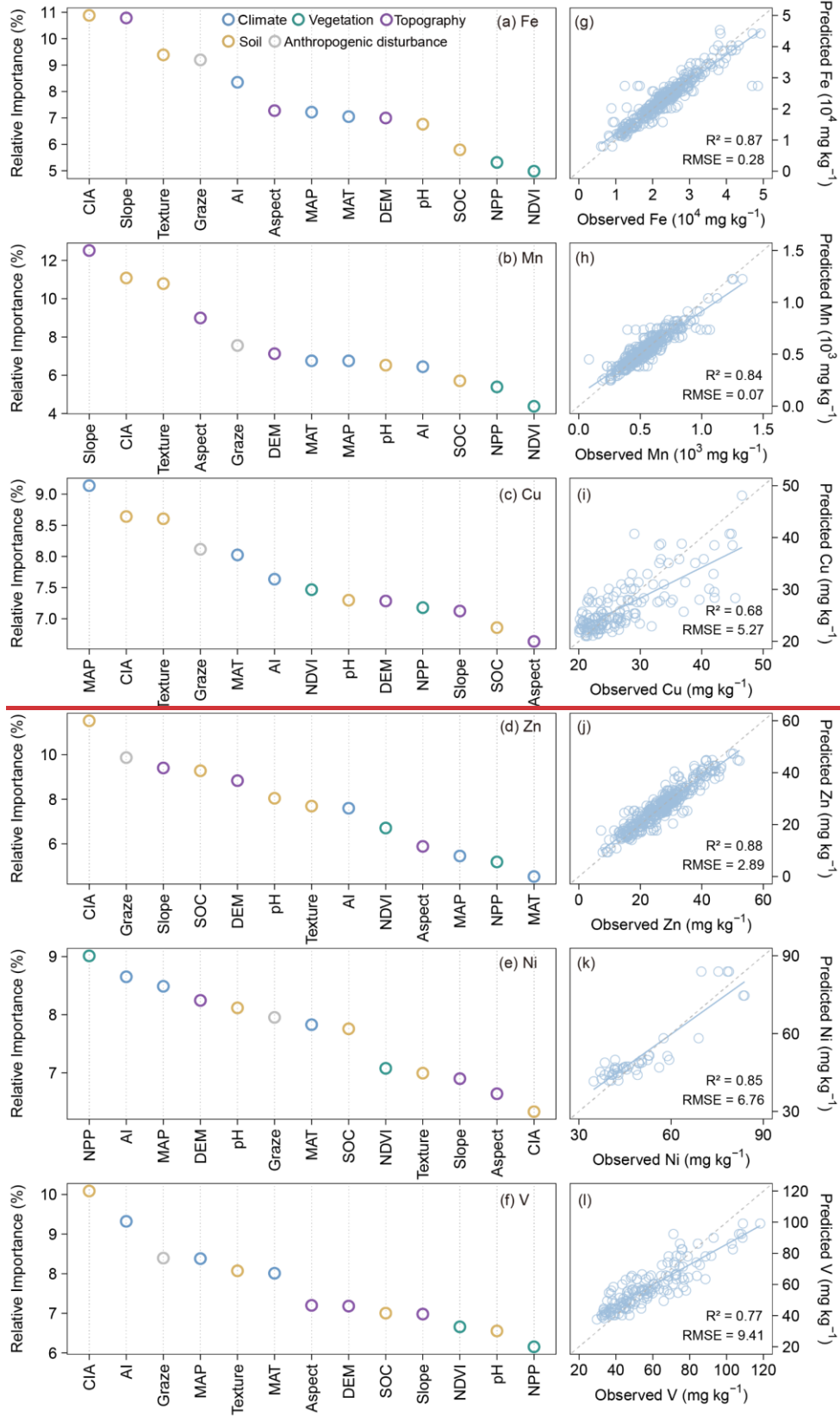
Soil Ni contents showed the most pronounced variation among lithologies, with the highest level recorded under acidic metamorphic rocks (64.43 mg kg^{-1}), followed by acidic igneous rocks (51.49 mg kg^{-1}). Soils developed from clastic sedimentary rocks and carbonate rocks had significantly lower Ni contents (45.85 and 41.06 mg kg^{-1} , respectively). The highest V contents were found in soils derived from acidic metamorphic rocks (63.67 mg kg^{-1}), followed by soils developed from eolian facies rocks (61.81 mg kg^{-1}) and fluvial facies rocks (55.67 mg kg^{-1}). In contrast, soils originating from carbonate (54.20 mg kg^{-1}), acidic igneous (54.11 mg kg^{-1}), and clastic sedimentary rocks (52.92 mg kg^{-1}) exhibited relatively lower V levels. In summary, Fe, Mn, Zn and V were substantially enriched in soils derived from acidic metamorphic rocks. Cu and Mo showed relatively uniform distributions across lithologies, Ni was notably elevated under acidic metamorphic rocks.

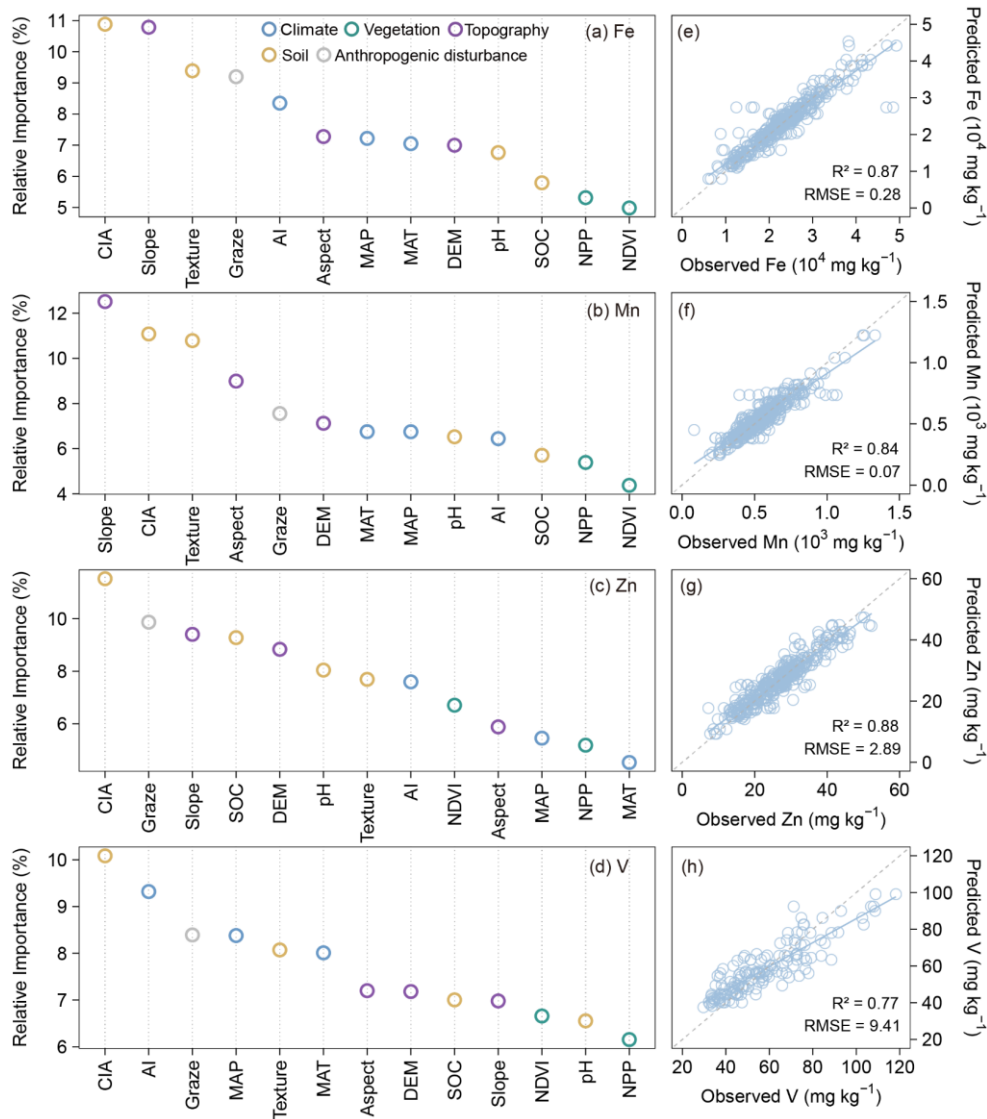
3.4 Drivers of soil micronutrient pattern

Relative importance analysis was conducted for five predictor groups, including climate, vegetation, soil covariates properties, topography, and grazing disturbances. The rankings show clear element-specific controls (Figs. 5a-da-f and S8). Soil covariates properties were the primary contributors to the spatial variation of micronutrient contents, followed by topographic and climatic factors, whereas vegetation and anthropogenic disturbance had relatively minor effects. Among all predictors,

283 ~~the chemical index of alteration~~CIA, slope, and soil texture exhibited the highest importance, indicating that weathering
284 intensity, terrain, and soil physical structure are the dominant controls on the spatial distribution of soil micronutrients.
285 Specifically, ~~the chemical index of alteration~~CIA emerged as the dominant factor for Fe, Zn, and V. Topographic factors
286 (slope) primarily influenced Mn, ~~while climatic variables (MAP, AI) and biological productivity (NPP) contributed more to~~
287 ~~Cu and Ni variations. Mo is mainly influenced by the soil texture.~~

288 The partial dependence plots illustrated the nonlinear responses of ~~seven~~four soil micronutrients (Fe, Mn, ~~Cu, Zn, Ni,~~and V,
289 ~~and Mo~~) to five key environmental variables (**Figs. 6 and S9**). ~~Overall, the effects of CIA, soil texture, slope, and moisture~~
290 ~~varied substantially among elements. Overall, the effects of the chemical index of alteration, soil texture, slope, and aridity~~
291 ~~index varied substantially among elements. The chemical index of alteration~~CIA showed a generally positive relationship
292 with most micronutrients, ~~particularly Fe, Mn, Zn, V, and Mo,~~ which increased markedly when chemical index of alteration
293 exceeded approximately 0.5. Soil texture exerted a moderate positive influence on micronutrients. In contrast, slope
294 exhibited a saturating effect—nutrient concentrations rose sharply at low slope angles (<10°) and plateaued
295 thereafter—highlighting the limited accumulation potential on steeper terrains. The aridity index demonstrated a clear
296 U-shaped pattern for most micronutrients ~~(Fe, Mn, Cu, Zn, Ni, V, and Mo),~~ with relatively low concentrations under
297 intermediate aridity. ~~Seven~~Four micronutrients ~~(Fe, Mn, Cu, Zn, Ni, V, and Mo)~~ exhibited a typical U-shaped relationship
298 with mean annual precipitation, showing higher contents in both low and high precipitation zones, and a clear trough in the
299 intermediate range (approximately 300-500 millimeters). This pattern aligned closely with responses to drought indices,
300 confirming shared moisture sensitivity. Collectively, these patterns emphasize that soil micronutrient distributions across the
301 Tibetan Plateau are strongly shaped by interactions among chemical weathering intensity, soil physical properties, and
302 climatic aridity.





304

305

306

307

308

Figure 5. Relative importance of biotic and abiotic factors for soil micronutrients (Fe, Mn, ~~Cu~~, Zn, ~~Ni~~, V) on the Tibetan Plateau (a-d). Relationship between observed and predicted values of soil micronutrients (Fe, Mn, ~~Cu~~, Zn, ~~Ni~~, V) on the Tibetan Plateau based on the Random Forest model (e-h). The blue solid line represents the fitted relationship using ordinary least squares regression, while the gray dashed line indicates the 1:1 line between observed and predicted values.

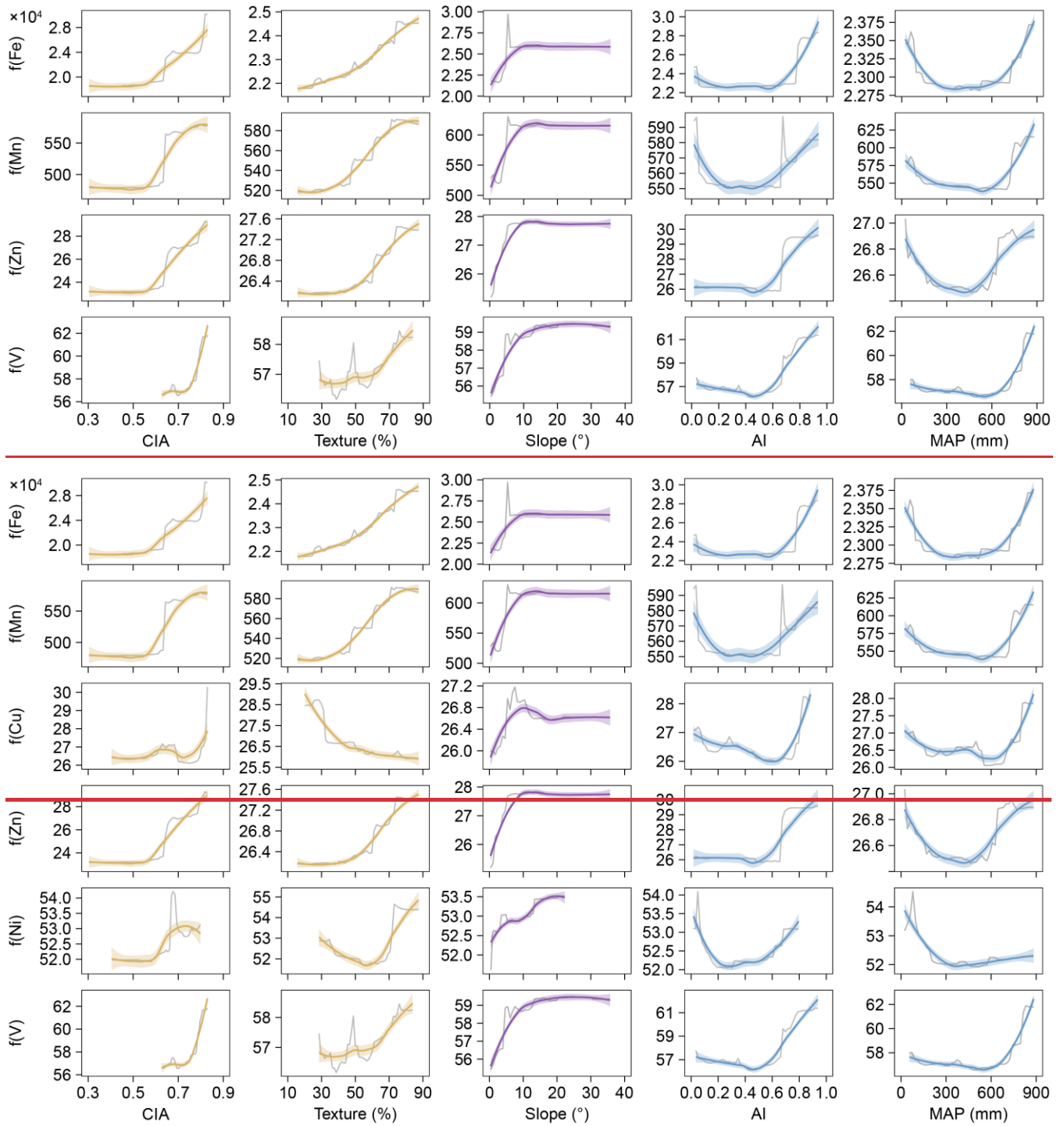


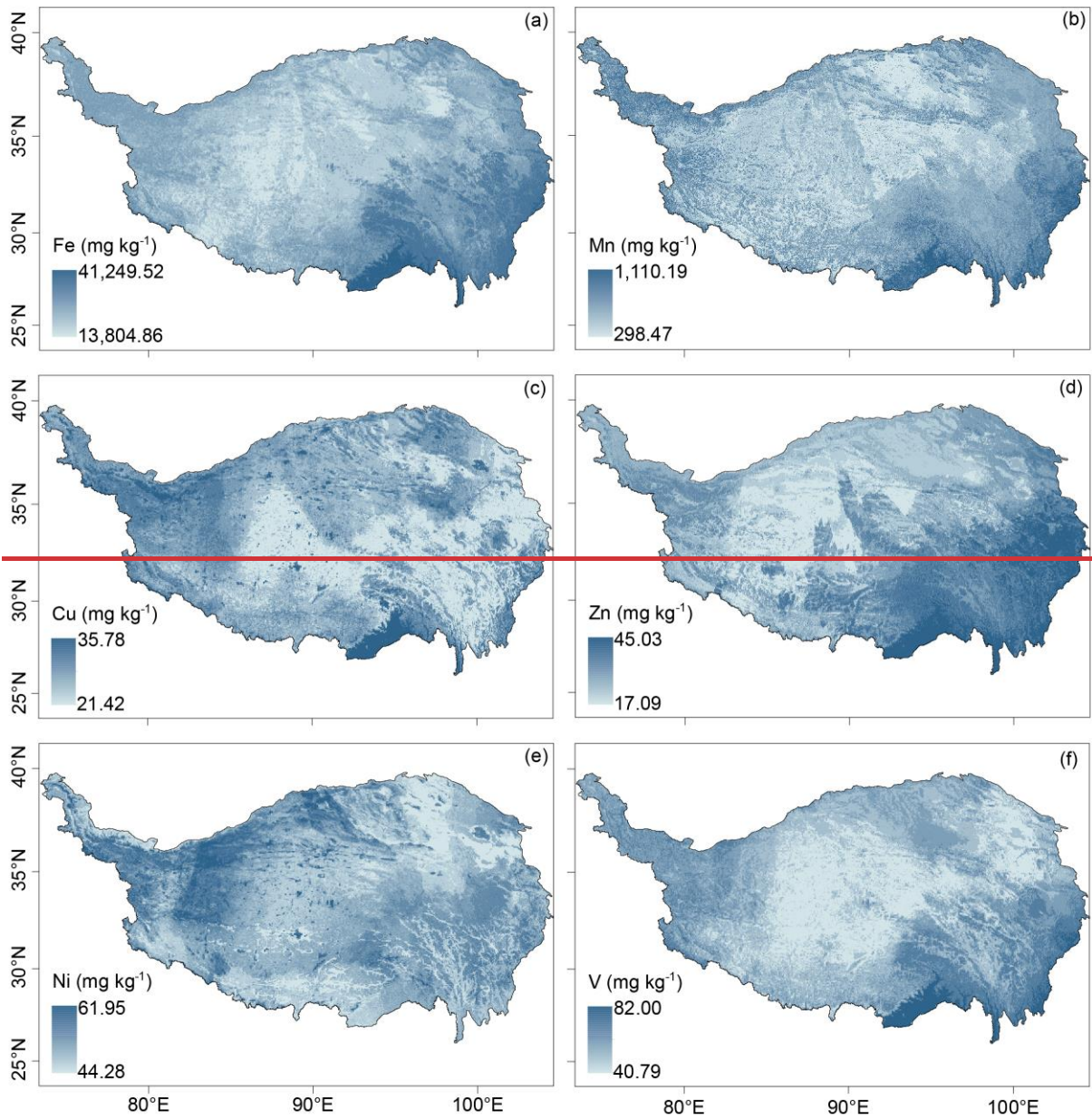
Figure 6. Partial dependence of ~~four~~ soil micronutrients (Fe, Mn, ~~Cu~~, Zn, Ni, V) on ~~five~~ predictive variables: chemical index of alteration (CIA), Texture, Slope, aridity index (AI) and mean annual precipitation (MAP). Gray lines represent the original partial dependence, while smoothed fits for each micronutrient are shown as colored lines. Shaded areas represent the 95% confidence intervals.

3.5 Soil micronutrients maps

The random forest (RF) models exhibited strong overall predictive performance for soil micronutrient ~~concentrations~~ ~~contents~~ across the Tibetan Plateau, with varying accuracies among elements (Figs. ~~5g5c-1~~ and S8). The models for Fe, Mn, and Zn, Ni, and Mo performed best, with R^2 values ranging from 0.843 to 0.88 and relatively low RMSE, indicating high

318 consistency between observed and predicted values. In particular, Zn ($R^2 = 0.88$) and Fe ($R^2 = 0.87$) achieved the highest
319 predictive accuracy, suggesting that their spatial variability is well captured by the selected environmental predictors. ~~Mo (R^2
320 $= 0.83$), Mn ($R^2 = 0.84$) and Ni ($R^2 = 0.85$)~~ also showed strong model fits, reflecting robust representation of their spatial
321 patterns. The ~~Cu and V~~ models displayed slightly lower but still acceptable performance ($R^2 = 0.68$ and 0.77 , respectively),
322 implying that additional predictors may be required to fully capture their local variability. Overall, these results demonstrate
323 that the random forest models effectively predict the spatial distributions of major soil micronutrients, with particularly high
324 reliability for Fe, Mn, ~~and Zn, and Ni~~.

325 **Figure 7 and Figure S10** illustrates the spatial patterns of soil micronutrients (Fe, Mn, ~~Cu, Zn, Ni, and V, and Mo~~) across the
326 Tibetan Plateau, as predicted by random forest models. The resulting maps reveal significant spatial heterogeneity of these
327 elements. The highest contents of Fe are primarily located in the southeastern region, the southern margins, and parts of the
328 western plateau. Mn shows a distinct gradient, with contents increasing from northeast to southwest. Predicted Mn values
329 range from 298.47 to 1,110.19 $\text{mg}\cdot\text{kg}^{-1}$, and the areas with the highest Mn contents are mainly distributed in the humid
330 southeastern and southern parts of the plateau. ~~Cu ranges from 21.42 to 35.78 $\text{mg}\cdot\text{kg}^{-1}$, with relatively higher contents over
331 the western northern interior and highlands and lower values in the humid southeastern valleys and along the southern
332 margin. Zn displays relatively high contents in the central-eastern region and along certain western edges of the plateau, with
333 predicted values ranging from 17.09 to 45.03 $\text{mg}\cdot\text{kg}^{-1}$. Ni has a narrower predicted content range (44.28–61.95 $\text{mg}\cdot\text{kg}^{-1}$) and
334 shows a more spatially homogeneous distribution. However, localized hotspots of elevated Ni contents are observed in parts
335 of the northeastern and southern plateau. Predicted V contents ranged from 40.79 to 82.00 $\text{mg}\cdot\text{kg}^{-1}$, displaying a clear spatial
336 gradient. Higher contents were predominantly found in the southeastern and southern regions of the plateau, where humid
337 climatic conditions and intense chemical weathering promote V enrichment. Moderate levels occurred across the central and
338 eastern plateau, while the lowest concentrations were observed in the arid western and northern areas. ~~In contrast, Mo varies
339 within a narrower interval (3.88–5.87 $\text{mg}\cdot\text{kg}^{-1}$) and exhibits a weak plateau wide gradient, with slight enrichment on the
340 northern plateau/basin areas and comparatively lower levels toward the southeast.~~~~



342

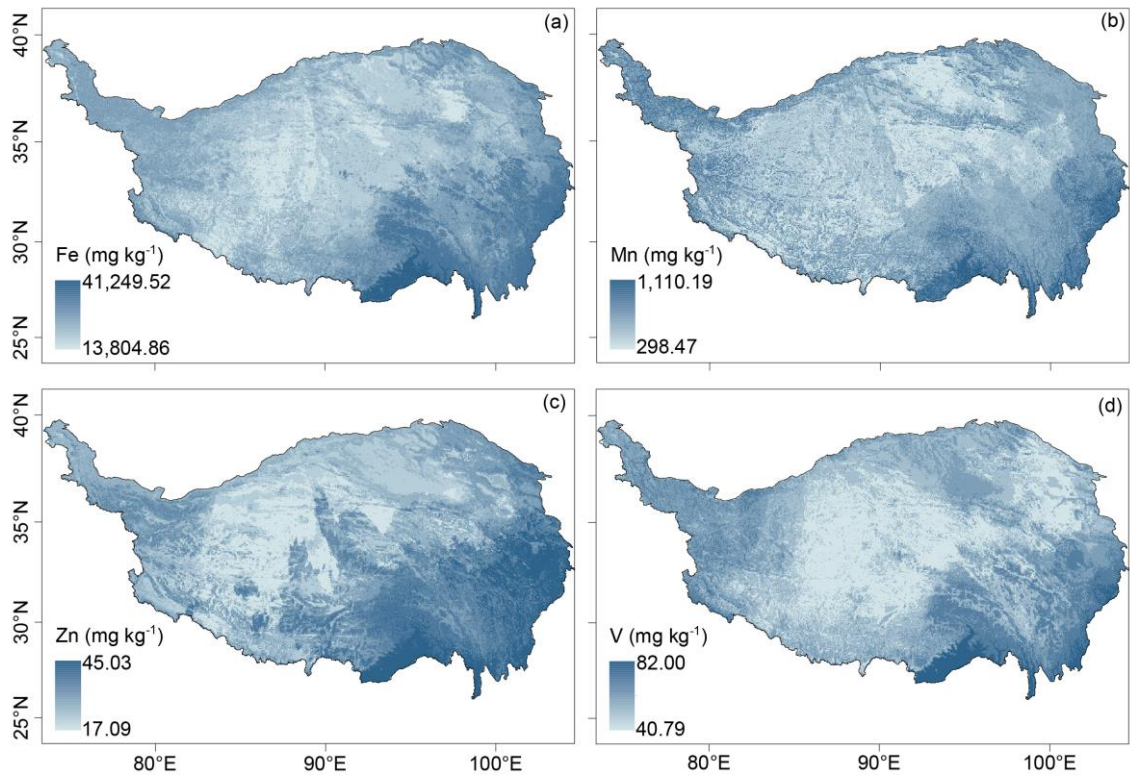


Figure 7. Spatial distribution of soil micronutrients (Fe, Mn, ~~Cu~~, Zn, ~~Ni~~, V) on the Tibetan Plateau.

4 Discussion

We added comparisons of our results with the few available observations on the Tibetan Plateau, as well as broader datasets from other regions, to better place our findings in a wider context (Table S1S2). In terms of data range and mean values, the contents and magnitudes of the soil micronutrients we observed are generally consistent with previous reports from the Plateau and global grassland soils, indicating the reliability of our datasets. For the Plateau, the mean Zn, and V contents in this study were slightly lower, ~~while Ni were somewhat higher~~ (Fig. S1S2). These discrepancies are more likely due to differences in study regions. Our sampling covered a much broader area, whereas previous studies focused mainly on local regions such as the Heihe Basin (Bu et al., 2016). Given the substantial spatial heterogeneity of soil micronutrients across the Tibetan Plateau, such differences are expected and further highlight the necessity of exploring soil micronutrient patterns at the plateau scale.

The vegetation-type contrasts likely reflect ecosystem controls on topsoil (0-10 cm) geochemistry (Fig. 3). These contrasts are consistent with ecosystem-mediated controls on topsoil geochemistry, where denser vegetation generally enhances near-surface nutrient cycling through greater biomass inputs, rhizosphere processes, and organic matter accumulation (Hinsinger, 2000). Increased organic inputs and reactive organo-mineral associations can promote retention of Fe, Mn, and Zn and, indirectly, V that is often associated with Fe-bearing phases (Lehmann et al., 2015). In contrast, arid steppe and

360 desert systems typically exhibit weaker soil development and lower organic inputs, reducing reactive surfaces and binding
361 sites for micronutrients, resulting in lower surface pools (Kabata-Pendias, 2010). Cropland tends to show intermediate levels,
362 likely reflecting mixing within the plough layer and partial homogenization of surface concentrations (Alloway, 2008).
363 Lithological class imposes a first order control on surface soil micronutrient variability (Fig. 4), consistent with the
364 well-established role of parent material in determining baseline micronutrient pools through differences in primary mineral
365 assemblages and weathering products. In our dataset, acidic metamorphic-derived soils are consistently enriched in Fe, Mn,
366 Zn, and V relative to several other lithologies, whereas acidic igneous and fluvial facies substrates tend to show lower
367 contents, with carbonate, eolian facies, and clastic sedimentary rocks generally occupying intermediate levels. Such contrasts
368 are expected where lithology governs not only the supply of Fe and Mn-bearing minerals but also the abundance of
369 secondary oxides and clay surfaces formed during pedogenesis, which strongly influence trace-element retention and
370 depletion intensity at regional scales (Lara et al., 2018; Spinola et al., 2022). The coherent behaviour of V alongside Fe is
371 also mechanistically plausible because vanadate is efficiently retained by Fe and Mn oxides, making V distributions closely
372 coupled to the abundance and reactivity of these mineral phases (Abernathy et al., 2022; Larsson et al., 2017).

373 The distribution of soil micronutrients across the Tibetan Plateau demonstrates significant spatial heterogeneity (**Figs. 2 and 7, S4, and S10**), aligning with patterns observed in Europe for elements such as Zn (Van et al., 2023). This variability is
374 predominantly governed by the interactions among soil, topography, and climate (**Figs. 5a-df and 6-S8 and S9**). Soils act as
375 the principal sink for micronutrients entering the terrestrial environment through both natural processes and anthropogenic
376 inputs. Consistent with continental-scale assessments, clay content emerged as the dominant control on the spatial
377 distribution of soil Zn in Europe, with coarse-textured soils showing markedly lower Zn concentrations (Van et al., 2023).
378 Similar texture effects have been reported for other elements: soil Cu is positively related to clay and negatively related to
379 sand (Ballabio et al., 2018), sensitivity analyses show that soil Se increases with increasing clay (Jones et al., 2017), whereas
380 surface-soil Hg decreases once sand exceeds ~30 % (Ballabio et al., 2021). These patterns agree with our observation that
381 ecosystems developed on coarse substrates contain the lowest levels of micronutrients. This is because clay serves as an
382 adsorption site for metal elements, whereas sandy soils are relatively weak adsorbents for micronutrients (Mesquita, 1998).
383 In poorly developed soils with low clay content, such as those in arid climates, the lack of capacity to retain soil organic
384 matter leads to a significant reduction in the amount of micronutrients, making them less likely to accumulate
385 (Moreno-Jimenez et al., 2019). In addition to soil covariates properties, factors such as topography also play a significant role
386 in the micronutrient content of surface soils on the Tibetan Plateau. Accumulated local effect (ALE) curves indicate
387 pronounced, nonlinear elevation responses in soil micronutrients, with Fe and Mn generally decreasing with elevation,
388 whereas Zn and V show threshold-like behaviour, remaining relatively stable at mid-elevations but changing sharply at
389 high elevations.

390 ~~higher elevations. Elevation related variations in soil micronutrient are limited, and some elements (e.g., Cu, Mo) remain~~
391 ~~relatively stable; Fe, Mn, Zn, and V show similar patterns, with higher contents at lower elevations than at higher ones (Fig.~~
392 ~~S12 and S13).~~ Contents of Fe, Mn, Zn, and V increased with slope steepness, particularly below 10°, ~~whereas Cu and Ni~~
393 ~~showed weaker or nonlinear trends.~~ This pattern suggests that topography governs both physical and chemical soil-forming
394 processes by controlling erosion, leaching, and moisture dynamics (Jenny, 1941; Montgomery, 2007). Steeper slopes
395 enhance runoff and erosion, removing fine particles enriched in Fe and Mn oxides and promoting elemental redistribution
396 along hillslopes, while also accelerating bedrock weathering and releasing lithogenic elements such as Fe and V (Yoo et al.,
397 2006). In contrast, gentler slopes favor organic matter accumulation and reducing conditions that can immobilize or leach
398 redox-sensitive elements. Overall, slope-driven variations in hydrology, weathering, and redox status collectively shape the
399 spatial heterogeneity of soil micronutrients across the Plateau (Quesada et al., 2010).

400 Notably, precipitation emerges as the primary predictor for micronutrients such as Fe, Mn, ~~Cu, Zn, and V, and Mo,~~ with all
401 elements exhibiting characteristic U-shaped responses, with minima occurring at 300-500 mm. This pattern likely reflects
402 distinct weathering regimes across precipitation gradients. In arid regions (<300 mm), physical weathering processes,
403 including freeze-thaw fracturing and aeolian erosion, predominate, allowing micronutrients ~~(e.g., Ni)~~ to accumulate near the
404 surface due to evaporation effects (Pachauri et al., 2014; Moreno-Jimenez et al., 2023). In transitional precipitation regimes
405 (300-500 mm), intensified chemical weathering occurs; however, leaching fluxes surpass the rates of parent material
406 weathering, leading to soil elemental depletion (Anderson, 2019; Bluth et al., 1994; Hartmann et al., 2014). In humid regions
407 (>500 mm), enhanced chemical weathering results in the formation of secondary clay minerals (e.g., montmorillonite, illite),
408 whose ~~negatively~~ charged surfaces facilitate elemental retention through ionic adsorption and co-precipitation mechanisms
409 (Alloway, 2009). To further verify these nonlinear effects, accumulated local effects ~~(ALE)~~ analyses were performed and
410 revealed consistent U-shaped responses for Fe, Mn, ~~Cu, Zn, and V, and Mo,~~ confirming the robustness of the partial
411 dependence results (Figs. S14 and S15). This pattern likely reflects a trade-off between weathering intensity, leaching losses,
412 and elemental retention under contrasting hydrological conditions. Additionally, MAP showed a significant positive
413 correlation with ~~the chemical index of alteration~~ CIA (Fig. S16S5), indicating that higher precipitation enhances chemical
414 weathering. However, this relationship alone does not fully explain the observed U-shaped nutrient responses, as direct
415 indicators of leaching fluxes and mineral retention are lacking. We therefore consider this U-shaped pattern, supported by
416 multiple lines of evidence, as an open question for future investigation, emphasizing the need for complementary datasets
417 (e.g., redox status, mineral composition) to refine its mechanistic interpretation. Although lithological differences are
418 detectable for some elements, they do not alter the overall spatial patterns (Figs. 4 and S7). In summary, lithology modulates
419 the baseline levels of certain micronutrients but is not the dominant factor shaping their regional distributions, which are

420 more strongly governed by external environmental drivers such as climate, weathering intensity, sediment transport, and
421 biotic cycling.

422 Our findings suggest that the aridity index is a significant determinant of soil micronutrient distribution. Specifically,
423 elemental contents tend to decrease when the aridity index falls below a certain threshold (**Figs. 6 and S9**). This trend likely
424 reflects reduced input or retention of elements under arid conditions. Grouped comparisons across aridity classes (humid, dry
425 sub-humid, semi-arid, arid, and hyper-arid) were performed. The results show that the medians and means of Fe, Mn, ~~Cu~~, Zn,
426 ~~Ni, and V, and Mo~~ decrease with increasing aridity, ~~with the largest declines observed for Fe, Mn, Zn, and V~~ (**Fig. S17 and**
427 **S18**). Drought conditions may modify soil redox states, thereby influencing element speciation, adsorption capacity,
428 mobility, and ultimately, leaching behavior (Brady et al., 2016; Loveland et al., 2003; Carter et al., 1995). Also, arid
429 environments may indirectly impact micronutrients through alterations in soil pH and soil organic matter content
430 (Moreno-Jimenez et al., 2019). Previous research has shown that droughts induced by climate change can restrict the
431 availability of essential micronutrients, such as iron and zinc ([Moreno-Jimenez et al., 2019](#); [Bista et al., 2018](#)). This
432 limitation, along with other adverse effects like diminished water availability, poses substantial threats to vital ecological
433 processes and services in drylands, including food production (Gupta et al., 2008; Graham, 1991). Furthermore, ongoing
434 regional warming and associated hydroclimatic shifts may interact with hydrology and redox processes, organic-matter
435 cycling, and vegetation patterns, thereby altering the availability and spatial variability of certain micronutrients (Myers et al.,
436 2014; Pachauri et al., 2014).

437 Multiple biogeochemical processes are sensitive to micronutrient availability. Biological nitrogen fixation relies on Mo and
438 Fe as essential cofactors of nitrogenase, while the methane cycle depends on Ni and Cu through their roles in
439 methanogenesis and methane oxidation, respectively (Thauer et al., 2019; Stefan et al., 2020). Permafrost thaw and
440 thermokarst development can further activate Fe-Mn redox cycling, altering metal mobility (Chauhan et al., 2024).
441 Collectively, soil micronutrients depletion may cascade through nutrient cycling and ecosystem feedbacks, amplifying the
442 impacts of ongoing environmental change across the Plateau.

443 **5 Uncertainty**

444 Although the laboratory XRF measurements used in this study were validated against ICP-MS and generally showed strong
445 correlations, several limitations should be noted. For Fe, Mn, ~~and V, and Cu~~, the two methods produced highly consistent
446 results, supporting the robustness of the dataset. In contrast, Zn ~~and Ni~~, exhibited systematic deviations from the 1:1 line,
447 with XRF tending to slightly ~~over- or~~ underestimate contents relative to ICP-MS (**Fig. S1**). These deviations likely arise

448 from element-specific detection sensitivities of XRF. To address this, we calibrated Zn ~~and Ni~~, using the regression
449 relationships between the two methods and then repeated spatial mapping. The results before and after calibration were not
450 significantly different, confirming that these deviations do not affect our main findings (**Figs. S2-S7 and S3-S8**). Furthermore,
451 the primary scientific purpose of this dataset is to characterize spatial patterns, ecological gradients, and multivariate
452 relationships across the Plateau, rather than to provide ultra-precise quantification of element contents at the
453 individual-sample level. For these objectives, XRF-derived contents, supported by calibration, cross-validation, and
454 transparent uncertainty reporting, provide reliable and ecologically interpretable information. For Mo, the results obtained
455 from the two methods were not fully consistent, likely due to its low content (Fig. S4). The XRF-based measurements may
456 involve considerable uncertainties. Nonetheless, we acknowledge that incorporating ICP-based measurements on a larger
457 sample set would further strengthen the accuracy of the dataset, and future efforts should consider combining multiple
458 analytical approaches to minimize methodological uncertainties.

459
460 Our random forest regression models demonstrated robust predictive capability (e.g. cross-validated R^2 range from 0.64-65
461 to 0.77 for Fe, Mn, and Zn-Ni; **Table S32**), Cu and Mo exhibit weaker predictive performance ($R^2 = 0.39$), which may be
462 attributed to the following reasons: First, analytical limitations may introduce measurement error, as both elements occur at
463 very low contents, especially Mo. Second, key process controls are not fully captured by the current predictors. E.g. Cu is
464 strongly influenced by nonlinear interactions with Fe/Al oxides, whereas Mo is affected by carbonate content, redox
465 conditions (Tack et al., 1995). These mineralogical and redox variables are underrepresented, leading to potential bias. In
466 addition, both elements show hotspot prone, right skewed distributions (Figs. 2 and S5), likely due to localized
467 anthropogenic sources. The spatial predictions inevitably contain uncertainties arising from both the Random Forest model
468 and the input datasets. Model-based uncertainty was quantified as the inter-tree variance among predictions (RF-SD; **Figs.**
469 **S11-S9 and S12**), while additional uncertainty may stem from sparse meteorological observations and limited soil sampling
470 across the Tibetan Plateau. Large regions in the west (including parts of the Changtang Plateau and Ngari) are sparsely
471 inhabited and difficult to access, with extensive high-elevation terrain and access restrictions that constrain fieldwork.
472 Consequently, model estimates in these areas are supported by fewer observations and should be interpreted with greater
473 caution. We therefore recommend that users consider the accompanying uncertainty layer when applying the gridded
474 products, especially for analyses focusing on the western Plateau or on fine-scale local interpretation. Nevertheless, model
475 accuracy could be further improved to more extensive field sampling and refinement of input data. Specifically, targeted
476 collection of soil micronutrient data and associated covariates in underrepresented high-altitude regions of the Tibetan
477 Plateau is necessary to address existing spatial gaps. Additionally, systematic reduction of uncertainties inherent in gridded

478 environmental datasets is essential, as these uncertainties propagate errors into micronutrient predictions. Continued
479 advancement in both field observations and foundational geospatial dataset is crucial for improving the reliability of
480 regional-scale element mapping.

481
482 We note that the reported contents represent a fixed-depth (0-10 cm) surface layer, which may correspond to different
483 dominant horizons among land uses (organic-rich surface in some forests, mineral topsoil in grasslands/meadows, and the
484 plough layer in croplands).~~We note that ecosystem-specific pedogenesis (e.g., organic rich surface layers in some forests vs.~~
485 ~~thin mineral A horizons in grasslands) can contribute to differences in surface micronutrient contents. Consequently, part of~~
486 ~~the spatial variation we report likely reflects vertical horizon contrasts sampled at a uniform 0-10 cm depth.~~ Users should
487 consider this context when applying the dataset, especially for process inference or when comparing across ecosystems with
488 contrasting surface horizons. Where applications require deeper profiles or horizon-specific interpretation, we recommend
489 integrating our maps with local profile data. Because croplands occupy a very small fraction of the Plateau and are
490 represented by a limited number of samples in our area-weighted design, cropland-related results should be interpreted
491 primarily as a cross-ecosystem contrast at the plateau scale. Users addressing cropland-specific questions are advised to use
492 these values with caution and, where possible, complement them with targeted cropland sampling or independent field
493 observations.

494

495 **6 Data availability**

496 The gridded soil micronutrient (Fe, Mn, ~~Cu~~, Zn, ~~Ni~~, and ~~V~~, and ~~Mo~~) maps for Tibetan Plateau can be downloaded from
497 <https://doi.org/10.11888/Terre.tpd.303049-303242> (Huo et al., 2025).

498 **7 Conclusions**

499 This study delivers a comprehensive assessment of spatial distribution patterns for ~~seven~~four soil micronutrients (Fe, Mn,
500 ~~Cu~~, Zn, ~~Ni~~, and ~~V~~, and ~~Mo~~) across the Tibetan Plateau, revealing pronounced regional-scale heterogeneity. Soil
501 ~~covariates~~properties were the primary contributors to the spatial variation of micronutrient contents, followed by topographic
502 and climatic factors, whereas vegetation and grazing disturbance had relatively minor effects. These findings highlight the
503 coupled effects of climate, vegetation, and parent material on micronutrient biogeochemical cycling within the complex
504 environmental context of the Tibetan Plateau. Using five predictor groups (climate, vegetation, soil covariates~~properties~~,

505 topography, and grazing disturbances), we generated high-resolution spatial maps for key soil micronutrients (Fe, Mn, ~~Cu~~,
506 Zn, ~~Ni~~, and ~~V~~, and ~~Mo~~) via machine learning. These maps provide validated initial conditions for process-based models
507 simulating micronutrient cycling, advances understanding of elemental distribution in alpine ecosystems.

508 ~~Author contributions.~~

509 ~~JZ conceived the study. HY conducted the field survey and was responsible for data collection and processing. HY prepared~~
510 ~~the manuscript with contributions from all co-authors.~~

511 Author contributions.

512 JZ conceived the study. HY conducted the field survey and was responsible for data collection and processing. HY prepared
513 the manuscript with contributions from all co-authors.

514 **Competing interests.**

515 The contact author has declared that none of the authors has any competing interests.

516 **Acknowledgements.**

517 This study was supported by the Second Tibetan Plateau Scientific Expedition and Research Program (2022QZKK0101),
518 National Natural Science Foundation of China (42471159), and Chinese Academy of Sciences (CAS) Project for Young
519 Scientists in Basic Research (YSBR-037).

520 **Appendix A: Supplementary material**

521 **Appendix B: Metadata**

522 **References**

523 [Abernathy, M. J., Schaefer, M. V., Ramirez, R., Garniwan, A., Lee, I., Zaera, F., Polizzotto, M. L., and Ying, S. C.: Vanadate](#)
524 [retention by iron and manganese oxides, ACS Earth and Space Chemistry, 6, 2041-2052,](#)
525 [https://doi.org/10.1021/acsearthspacechem.2c00116, 2022.](https://doi.org/10.1021/acsearthspacechem.2c00116)
526 [Alloway, B. J.: Zinc in soils and crop nutrition, 2nd edn., International Zinc Association \(IZA\) and International Fertilizer](#)
527 [Industry Association \(IFA\), Brussels and Paris, 2008.](#)

528 Alloway, B. J.: Soil factors associated with zinc deficiency in crops and humans, *Environmental Geochemistry and Health*,
529 31, 537-548, <https://doi.org/10.1007/s10653-009-9255-4>, 2009.

530 Anderson, S. P.: Breaking it down: Mechanical processes in the weathering engine, *Elements: An International Magazine of*
531 *Mineralogy, Geochemistry, and Petrology*, 15, 247-252, <https://doi.org/10.2138/gselements.15.4.247>, 2019.

532 Bluth, G. J., and Kump, L. R.: Lithologic and climatologic controls of river chemistry, *Geochimica et Cosmochimica Acta*,
533 58, 2341-2359, [https://doi.org/10.1016/0016-7037\(94\)90015-9](https://doi.org/10.1016/0016-7037(94)90015-9), 1994.

534 Ballabio, C., Jiskra, M., Osterwalder, S., Borrelli, P., Montanarella, L., and Panagos, P.: A spatial assessment of mercury
535 content in the European Union topsoil, *Science of the Total Environment*, 769, 144755, [https://doi.org/](https://doi.org/10.1016/j.scitotenv.2020.144755)
536 [10.1016/j.scitotenv.2020.144755](https://doi.org/10.1016/j.scitotenv.2020.144755), 2021.

537 Ballabio, C., Panagos, P., Lugato, E., Huang, J. H., Orgiazzi, A., Jones, A., Fernández-Ugalde, O., Borrelli, P., and
538 Montanarella, L.: Copper distribution in European topsoils: An assessment based on LUCAS soil survey, *Science of the*
539 *Total Environment*, 636, 282-298, <https://doi.org/10.1016/j.scitotenv.2018.04.268>, 2018.

540 [Bista, D. R., Heckathorn, S. A., Jayawardena, D. M., Mishra, S., and Boldt, J. K.: Effect of drought and carbon dioxide on](https://doi.org/10.1002/ajb2.1542)
541 [nutrient uptake and levels of nutrient-uptake proteins in roots of barley, *American Journal of Botany*, 107, 1401-1409,](https://doi.org/10.1002/ajb2.1542)
542 [https://doi.org/ 10.1002/ajb2.1542](https://doi.org/10.1002/ajb2.1542), 2018.

543 Brady, N. C. and Weil, R. R.: *The nature and properties of soils*, Pearson Education, Boston, 1104 pp., 2016.

544 Bu, J. W., Sun, Z. Y., Zhou, A. G., Xu, Y. N., Ma, R., Wei, W. H., and Liu, M.: Heavy Metals in Surface Soils in the Upper
545 Reaches of the Heihe River, Northeastern Tibetan Plateau, China, 13, [https://doi.org/ 10.3390/ijerph13030247](https://doi.org/10.3390/ijerph13030247), 2016.

546 [Cardon, Z. G., Stark, J. M., Herron, P. M., and Rasmussen, J. A.: Sagebrush carrying out hydraulic lift enhances surface soil](https://doi.org/10.1073/pnas.1311314110)
547 [nitrogen cycling and nitrogen uptake into inflorescences, *Proceedings of the National Academy Sciences of the United*](https://doi.org/10.1073/pnas.1311314110)
548 [States of America](https://doi.org/10.1073/pnas.1311314110), 110, 18988-18993, <https://doi.org/10.1073/pnas.1311314110>, 2013.

549 Carter, M. R. and Stewart, B. A.: *Structure and organic matter storage in agricultural soils*, CRC Press, Boca Raton, 304 pp.,
550 1995.

551 Chauhan, A., Patzner, M. S., Bhattacharyya, A., Borch, T., Fischer, S., Obst, M., Thomasarrigo, L. K., Kretzschmar, R.,
552 Mansor, M., Bryce, C., Kappler, A., and Joshi, P.: Interactions between iron and carbon in permafrost thaw ponds,
553 *Science of the Total Environment*, 946, 174321, <https://doi.org/10.1016/j.scitotenv.2024.174321>, 2024.

554 Cheng, C. J., He, N. P., Li, M. X., Xu, L., Cai, W. X., Li, X., Zhao, W. W., Li, C., and Sun, O. J.: Plant species richness on
555 the Tibetan Plateau: patterns and determinants, *Ecography*, 2023, <https://doi.org/10.1111/ecog.06265>, 2022.

556 [Cheng, F. T., Chen, D. L., Wang, B., Ou, T. H., and Lu, M. Q.: Human-induced warming accelerates local evapotranspiration](#)
557 [and precipitation recycling over the Tibetan Plateau, *Communications Earth Environment*, 388,](#)
558 <https://doi.org/10.1038/s43247-024-01537-8>, 2024.

559 Chen, J. H., Wang, Y. F., Sun, J., Zhang, J. X., Zhang, J. T., Wang, Y. X., Zhou, T. C., Huo, H. Y., and Liang, E. Y.: Linking
560 ecosystem service benefit and grazing prohibition intensity can better optimize fence layout in northern Tibet, *Land*
561 *Degradation Development*, 34, 2038-2051, <https://doi.org/10.1002/ldr.4587>, 2023.

562 Dallman, P. R.: Biochemical basis for the manifestations of iron deficiency, *Annual Review of Nutrition*, 6, 13-40,
563 <https://doi.org/10.1146/annurev.nu.06.070186.000305>, 1986.

564 Dijkshoorn, J. A., van Engelen, V. W. P., and Huting, J. R. M.: Soil and landform properties for LADA partner countries
565 (Argentina, China, Cuba, Senegal and The Gambia, South Africa and Tunisia), ISRIC Report 2008/06 and GLADA
566 Report 2008/03, ISRIC-World Soil Information and FAO, Wageningen, 23 pp., 2008.

567 Dijkstra, J. J., Meeussen, J. C. L., and Comans, R. N. J.: Leaching of heavy metals from contaminated soils: an experimental
568 and modeling study. *Environmental Science & Technology*, 38, 4390-4395, <https://doi.org/10.1021/es049885v>, 2004.

569 [Dong, K., Li, W. J., Tang, Y. L., Ma, S. H., and Jiang, M. L.: Co-limitation of N and P is more prevalent in the](#)
570 [Qinghai-Tibetan Plateau grasslands, *Frontiers in Plant Science*, 14, 1140462, https://doi.org/10.3389/fpls.2023.1140462,](#)
571 [2023.](#)

572 [Du, Z. Y., Cai, Y. J., Yan, Y., and Wang, X. D.: Embedded rock fragments affect alpine steppe plant growth, soil carbon and](#)
573 [nitrogen in the northern Tibetan Plateau, *Plant and Soil*, 420, 79-92, https://doi.org/10.1007/s11104-017-3376-9, 2017.](#)

574 Fageria, N. K., Baligar, V. C., and Clark, R. B.: Micronutrients in crop production. *Advances in Agronomy*, 77, 185-268,
575 [https://doi.org/10.1016/S0065-2113\(02\)77015-6](https://doi.org/10.1016/S0065-2113(02)77015-6), 2002.

576 Fedo, C. M., Nesbitt, H. W., and Young, G. M.: Unraveling the effects of potassium metasomatism in sedimentary rocks and
577 paleosols, with implications for paleoweathering conditions and provenance, *Geology*, 23, 921-924,
578 [https://doi.org/10.1130/0091-7613\(1995\)023<0921:UTEOPM>2.3.CO;2](https://doi.org/10.1130/0091-7613(1995)023<0921:UTEOPM>2.3.CO;2), 1995.

579 Fischer, W. W., Hemp, J., and Johnson, J. E.: Manganese and the evolution of photosynthesis, *Origins of Life and Evolution*
580 *of Biospheres*, 45, 351-357, <https://doi.org/10.1007/s11084-015-9442-5>, 2015.

581 Graham, T. W.: Trace element deficiencies in cattle, *Veterinary Clinice of North America-Food Animal Practice*, 7, 153-215,
582 [https://doi.org/10.1016/S0749-0720\(15\)30816-1](https://doi.org/10.1016/S0749-0720(15)30816-1), 1991.

583 Gupta, U. C., Wu, K., and Liang, S.: Micronutrients in soils, crops, and livestock. *Earth Science Frontiers*, 15, 110-125,
584 2008.

585 Guan, Z. H., Li, X. G., and Wang, L.: Heavy metal enrichment in roadside soils in the eastern Tibetan Plateau,
586 Environmental Science and Pollution Research, 25, 7625-7637, [https://doi.org/ 10.1007/s11356-017-1094-8](https://doi.org/10.1007/s11356-017-1094-8), 2017.

587 [Han, D. L., Huang, J. P., Ding, L., Zhang, G. L., Liu, X. Y., Li, C. Y., and Yang, F.: Breaking the Ecosystem Balance Over the](#)
588 [Tibetan Plateau, Earth's Future, 10, \[https://doi.org/ 10.1029/2022EF002890\]\(https://doi.org/10.1029/2022EF002890\), 2022.](#)

589 Hartmann, J., Moosdorf, N., Lauerwald, R., Hinderer, M., and West, A. J.: Global chemical weathering and associated
590 P-release-The role of lithology, temperature and soil properties, Chemical Geology, 363, 145-163,
591 <https://doi.org/10.1016/j.chemgeo.2013.10.025>, 2014.

592 Hartmann, M., and Six, J.: Soil structure and microbiome functions in agroecosystems, Nature Reviews Earth &
593 Environment, 4, 4-18, <https://doi.org/10.1038/s43017-022-00366-w>, 2023.

594 Hänsch, R., and Mendel, R. R.: Physiological functions of mineral micronutrients (Cu, Zn, Mn, Fe, Ni, Mo, B, Cl), Current
595 Opinion in Plant Biology, 12, 259-266, <https://doi.org/10.1016/j.pbi.2009.05.006>, 2009.

596 [Hinsinger, P.: Bioavailability of trace elements as related to root-induced changes in the rhizosphere. Trace Elements in the](#)
597 [Rhizosphere, 25-41, <http://dx.doi.org/10.1201/9781420039993.ch2>, 2001.](#)

598 Hou, X. Y. (Ed.): Atlas of vegetation of China (1:1,000,000), Science Press, Beijing, 2019.

599 Jenny, H.: Factors of Soil Formation: A System of Quantitative Pedology, McGraw-Hill, New York, 1941.

600 Jones, D. L., Cross, P., Withers, P. J., DeLuca, T. H., Robinson, D. A., Quilliam, R. S., Harris, I. M., Chadwick, D. R., and
601 Edwards-Jones, G.: Nutrient stripping: The global disparity between food security and soil nutrient stocks, Journal of
602 Applied Ecology, 50, 851-862, <https://doi.org/10.1111/1365-2664.12089>, 2013.

603 Jones, G. D., Droz, B., Greve, P., Gottschalk, P., Poffet, D., McGrath, S. P., Seneviratne, S. I., Smith, P., and Winkel, L. H. E.:
604 Selenium deficiency risk predicted to increase under future climate change, Proceedings of the National Academy of
605 Sciences of the United States of America, 114, 2848-2853, <https://doi.org/10.1073/pnas.1611576114>, 2017.

606 [Kabata-Pendias, A.: Trace elements in soils and plants, 4th edn., CRC Press, Boca Raton, FL, USA, 2011.](#)

607 [Lara, M. C., Buss, H. L., and Pett-Ridge, J. C.: The effects of lithology on trace element and REE behavior during tropical](#)
608 [weathering, Chemical Geology, 500, 88-1020, <https://doi.org/10.1016/j.chemgeo.2018.09.024>, 2018.](#)

609 [Larsson, M. A., Persson, I., Sjoestedt, C., and Gustafsson, J. P.: Vanadate complexation to ferrihydrite: X-ray absorption](#)
610 [spectroscopy and CD-MUSIC modelling, Environmental Chemistry, 14, 141-150, <https://doi.org/10.1071/EN16174>,](#)
611 [2017.](#)

612 [Lehmann, J., and Kleber, M.: The contentious nature of soil organic matter, Nature, 528, 60-68, \[https://doi.org/\]\(https://doi.org/10.1038/nature16069\)](#)
613 [10.1038/nature16069](#), 2015.

614 Lemièrè, B.: A review of pXRF (field portable X-ray fluorescence) applications for applied geochemistry, Journal of

615 Geochemical Exploration, 188, 350-363, <https://doi.org/10.1016/j.gexplo.2018.02.006>, 2018.

616 Lindsay, W. L.: Chemical equilibria in soils, John Wiley and Sons Ltd., New York, 449 pp., 1979.

617 Loveland, P. and Webb, J.: Is there a critical level of organic matter in the agricultural soils of temperate regions: a review,
618 Soil Tillage Research, 70, 1–18, [https://doi.org/10.1016/S0167-1987\(02\)00139-3](https://doi.org/10.1016/S0167-1987(02)00139-3), 2003.

619 McLennan, S. M.: Weathering and global denudation, The Journal of Geology, 101, 295-303, <https://doi.org/10.1086/648222>,
620 1993.

621 Mesquita, M. E.: Copper and zinc competitive adsorption in schistic and granitic acid soils, Agrochimica, 42, 235-245, 1998.

622 Montgomery, D. R.: Soil erosion and agricultural sustainability, Proceedings of the National Academy of Sciences of the
623 United States of America, 104, 13268-13272, <https://doi.org/10.1073/pnas.0611508104>, 2007.

624 Moreno-Jimenez, E., Maestre, F. T., Flagmeier, M., Guirado, E., Berdugo, M., Bastida, F., Dacal, M., Díaz-Martínez, P.,
625 Ochoa-Hueso, R., Plaza, C., Rillig, MC., Crowther, T. W., and Delgado-Baquerizo, M.: Soils in warmer and less
626 developed countries have less micronutrients globally, Global Change Biology, 29, 522-532,
627 <https://doi.org/10.1111/gcb.16478>, 2023.

628 Moreno-Jimenez, E., Plaza, C., Saiz, H., Manzano, R., Flagmeier, M., and Maestre, F. T.: Aridity and reduced soil
629 micronutrient availability in global drylands, Nature Sustainability, 2, 371-377,
630 <https://doi.org/10.1038/s41893--019-0262-x>, 2019.

631 Mu, C. C., Zhang, F., Mu, M., Chen, X., Li, Z. L., and Zhang, T. J.: Organic carbon stabilized by iron during slump
632 deformation on the Qinghai-Tibetan Plateau, Catena, 187, 104282, <https://doi.org/10.1016/j.catena.2019.104282>, 2020.

633 Mu, C. C., Zhang, T. J., Zhao, Q., Guo, H., Zhong, W., Su, H., and Wu, Q.B.: Soil organic carbon stabilization by iron in
634 permafrost regions of the Qinghai-Tibet Plateau, Geophysical Research Letters, 43, 10286-10294,
635 <https://doi.org/10.1002/2016GL070071>, 2016.

636 Myers, S. S., Zanobetti, A., Kloog, I., Huybers, P., Leakey, A. D., Bloom, A. J., Carlisle, E., Dietterich, L. H., Fitzgerald, G.,
637 Hasegawa, T., Holbrook, N. M., Nelson, R. L., Ottman, M. J., Raboy, V., Sakai, H., Sartor, K. A., Schwartz, J.,
638 Seneweera, S., Tausz, and M., Usui, Y.: Increasing CO₂ threatens human nutrition, Nature, 510, 139-142,
639 <https://doi.org/10.1038/nature13179>, 2014.

640 Nesbitt, H.W., and Young, G.M.: Early Proterozoic climates and plate motions inferred from major element chemistry of
641 lutites, Nature, 299, 715-717, <https://doi.org/10.1038/299715a0>, 1982.

642 Ochoa-Hueso, R., Plaza, C., Moreno-Jimenez, E., and Delgado-Baquerizo, M.: Soil element coupling is driven by ecological
643 context and atomic mass, Ecology Letters, 24, 319-326, <https://doi.org/10.1111/ele.13648>, 2020.

- 644 O'Hara, G. W.: Nutritional constraints on root nodule bacteria affecting symbiotic nitrogen fixation: A review, *Australian*
645 *Journal of Experimental Agriculture*, 41, 417-433, <https://doi.org/10.1071/EA00087>, 2001.
- 646 Pachauri, R. K., Allen, M. R., Barros, V. R., Broome, J., Cramer, W., Christ, R., Church, J. A., Clarke, L., Dahe, Q., and
647 Dasgupta, P.: Climate change 2014: Synthesis report. Contribution of Working Groups I, II and III to the Fifth
648 Assessment Report of the Intergovernmental Panel on Climate Change, IPCC, Geneva, Switzerland, 151 pp., 2014.
- 649 [Pan, J. X., Zhang, X. Y., Liu, S., Liu, N., Liu, M. J., Chen, C., Zhang, X. Y., Niu, S. L., and Wang, J. S.: Precipitation](#)
650 [alleviates microbial C limitation but aggravates N and P limitations along a 3000-km transect on the Tibetan Plateau,](#)
651 [Catena, 247, 108535, https://doi.org/10.1016/j.catena.2024.108535, 2024.](#)
- 652 Piñeiro, G., Perelman, S., Guerschman, J. P., and Paruelo, J. M.: How to evaluate models:: Observed vs. predicted or
653 predicted vs. observed? *Ecological Modelling*, 216, 316-322, <https://doi.org/10.1016/j.ecolmodel.2008.05.006>, 2008.
- 654 Potter, C. S., Randerson, J. T., Field, C. B., Matson, P. A., Vitousek, P. M., Mooney, H. A., and Klooster, S. A.: Terrestrial
655 ecosystem production: A process model based on global satellite and surface data, *Global Biogeochemical Cycles*, 7,
656 811–841, <https://doi.org/10.1029/93GB02725>, 1993.
- 657 Prestele, R., Alexander, P., Rounsevell, M. D., Arneth, A., Calvin, K., Doelman, J., Eitelberg, D. A., Engström, K., Fujimori,
658 S., Hasegawa, T., Havlik, P., Humpenoeder, F., Jain, A. K., Krisztin, T., Kyle, P., Meiyappan, P., Popp, A., Sands, R. D.,
659 Schaldach, R., Schuengel, J., Stehfest, E., Tabeau, A., Van Meijl, H., Van Vliet, J., Verburg, P. H.: Hotspots of
660 uncertainty in land-use and land-cover change projections: A global-scale model comparison, *Global Change Biology*,
661 22, 3967-3983, <https://doi.org/10.1111/gcb.13337>, 2016.
- 662 Quesada, C. A., Lloyd, J., Schwarz, M., Patino, S., Baker, T. R., Czimczik, C., Fyllas, N. M., Martinelli, L., Nardoto, G. B.,
663 Schmerler, J., Santos, A. J. B., Hodnett, M. G., Herrera, R., Luizao, F. J., Arneth, A., Lloyd, G., Dezzeo, N., Kuhlmann,
664 I., Raessler, M., Brand, W. A., Geilmann, H., Moraes Filho, J. O., Carvalho, F. P., Araujo Filho, R. N., Chaves, J. E.,
665 Cruz Junior, O. F., Pimentel, T. P., and Paiva, R.: Variations in chemical and physical properties of Amazon forest soils
666 in relation to their genesis, *Biogeosciences*, 7, 1515-1541, <https://doi.org/10.5194/bg-7-1515-2010>, 2010.
- 667 Schmidt, W., Thomine, S., and Buckhout, T. J.: Iron nutrition and interactions in plants, *Frontiers in Plant Science*, 10, 1670,
668 <https://doi.org/10.3389/fpls.2019.01670>, 2020.
- 669 Simon M. N.: *Inductively Coupled Plasma Mass Spectrometry Handbook*, Blackwell Publishing, Oxford, 2005.
- 670 [Spinola, D., Portes, R., Fedenko, J., Lybrand, R., Dere, A., Biles, F., Trainor, T., Bowden, M. E., and D'Amore, D.:](#)
671 [Lithological controls on soil geochemistry and clay mineralogy across Spodosols in the coastal temperate rainforest of](#)
672 [southeast Alaska, *Geoderma*, 428, 116211, https://doi.org/10.1016/j.geoderma.2022.116211, 2022.](#)

673 Stefan, B., Jiménez-Vicente, E., Echavarri-Erasun, C., and Rubio, L. M.: Biosynthesis of Nitrogenase Cofactors, *Chemical*
674 *Reviews*, 120, 4919-5794, <https://doi.org/10.1021/acs.chemrev.9b00489>, 2020.

675 Stehfest, E., van Zeist, W. J., Valin, H., Havlik, P., Popp, A., Kyle, P., Tabeau, A., Mason-D'Croz, D., Hasegawa, T., Bodirsky,
676 B. L., Calvin, K., Doelman, J. C., Fujimori, S., Humpenoeder, F., Lotze-Campen, H., van Meijl, H., and Wiebe, K.: Key
677 determinants of global land-use projections, *Nature Communications*, 10, 1-10,
678 <https://doi.org/10.1038/s41467-019-09945-w>, 2019.

679 St Clair, S. B. S., and Lynch, J. P.: The opening of Pandora's Box: Climate change impacts on soil fertility and crop nutrition
680 in developing countries, *Plant and Soil*, 335, <https://doi.org/10.1007/s11104-010-0328-z101-115>, 2010.

681 ~~Tack, F.M., Verloo M.G.: Chemical speciation and fractionation in soil and sediment heavy metal analysis: a review,~~
682 ~~*International Journal of Environmental Analytical Chemistry* 59, 225-238. <https://doi:10.1080/03067319508041330>,~~
683 ~~1995.~~

684 Thauer, P. K.: Methyl (Alkyl)-Coenzyme M Reductases: Nickel F-430-Containing Enzymes Involved in Anaerobic Methane
685 Formation and in Anaerobic Oxidation of Methane or of Short Chain Alkanes, *Biochemistry*, 58, 5198-5220.
686 <https://doi:10.1021/acs.biochem.9b00164>, 2019.

687 ~~Tian, L. M., Zhao, L., Wu, X. D., Hu, G. J., Fang, H. B., Zhao, Y. H., Sheng, Y., Chen, J., Wu, J. C., Li, W. P., Ping, C.L.,~~
688 ~~Pang, C. L., Pang, Q. Q., Liu, Y., Shi, W., Wu, T. H., and Zhang, X. M.: Variations in soil nutrient availability across~~
689 ~~Tibetan grassland from the 1980s to 2010s, *Geoderma*, 338, 197-205, <https://doi.org/10.1016/j.geoderma.2018.12.009>,~~
690 ~~2019.~~

691 Trabucco, A. and Zomer, R. J.: Global Aridity Index and Potential Evapo-Transpiration (ET₀) Climate Database v2, CGIAR
692 Consortium for Spatial Information (CGIAR-CSI) [data set], <https://cgiarcsi.community>, 2018.

693 Van, Eynde, E., Fendrich, A. N., Ballabio, C., and Panagos, P.: Spatial assessment of topsoil zinc concentrations in Europe,
694 *Science of the Total Environment*, 892, 164512, <https://doi.org/10.1016/j.scitotenv.2023.164512>, 2023.

695 White, P. J., and Broadley, M. R.: Biofortifying crops with essential mineral elements. *Trends in Plant Science*, 10, 586-593,
696 <https://doi.org/10.1016/j.tplan ts.2005.10.001>, 2005.

697 ~~Yao, T. D., Thompson, L. G., Mosbrugger, V., Zhang, F., Ma, Y. M., Luo, T. X., Xu, B. Q., Yang, X. X., Joswiak, D. R.,~~
698 ~~Wang, W. C., Joswisk, M. E., Devkota, L. P., Tayal, S., Jilani, R., Fayziev, R.: *Third Pole Environment (TPE),*~~
699 ~~*Environmental Development*, 3, 52-64, <https://doi.org/10.1016/j.envdev.2012.04.002>, 2012.~~

700 Yoo, K., Amundson, R., Mudd, S. M., Sanderman, J., Amundson, R., and Blum, A.: Spatial patterns and controls of soil
701 chemical weathering rates along a transient hillslope, *Earth and Planetary Science Letters*, 288, 184-193,
702 <https://doi.org/10.1016/j.epsl.2009.09.021>, 2006.

703 [Yu, Y. F., You, Q. L., Zhang, Y. Q., Jin, Z., Kang, S. C., and Zhai, P. M.: Integrated warm-wet trends over the Tibetan Plateau](#)
704 [in recent decades. Journal of Hydrology, 639, 131599, <https://doi.org/10.1016/j.jhydrol.2024.131599>, 2024.](#)

705 Zhang, H., Wang, Z. F., Zhang, Y. L., and Hu, Z. J.: The effects of the Qinghai-Tibet railway on heavy metals enrichment in
706 soils, Science of the Total Environment, 439, 240-280, <https://doi.org/10.1016/j.scitotenv.2012.09.027>, 2012.